A hidden sedimentary phosphate pool inside benthic foraminifera from the Peruvian upwelling region might nucleate phosphogenesis

N. Glock[1,*], D. Romero[2], A.-S. Roy[3], C. Woehle[3,4], A. W. Dale[1], J. Schönfeld[1], T. Wein[3], J. Weissenbach[3,5], and T. Dagan[3]

[1]: GEOMAR Helmholtz Centre for Ocean Research Kiel, Wischhofstrasse 1-3, 24148 Kiel, Germany

[2]: IMARPE, Dirección General de Investigaciones Oceanográficas y Cambio Climático, Callao 01, Peru

[3]: Institute of Microbiology, Kiel University, Am Botanischen Garten 11, 24118 Kiel, Germany

[4]: Present address: Max Planck-Genome-centre Cologne, Max Planck Institute for Plant Breeding Research, Cologne, Germany

[5]: Present address: Faculty of Biology, Technion – Israel Institute of Technology, Haifa, 3200003, Haifa, Israel

*: Correspondence to N. Glock (nglock@geomar.de)

Abstract

Phosphorus is essential for all living organisms, being a component of DNA and RNA and the energy carrier ATP. Phosphogenesis is a main sink of reactive phosphorus in the oceans. The present study reports the presence of intracellular dissolved inorganic phosphate (DIP) in benthic foraminifera from the Peruvian oxygen minimum zone (OMZ). The mean intracellular DIP concentration was 28 ± 3 mM; two to three orders-of-magnitude higher than in the ambient pore waters. The biological implications of the high intracellular phosphate enrichment may be related to the synthesis of polyphosphates or phospholipids for cell-membranes. The comparative genomics analysis of multiple species of foraminifera from different environments reveals that foraminifers encode the genes required for both phospholipid and polyphosphate metabolism. Rapid phosphogenesis and phosphorite formation associated with foraminiferal tests is hypothesized due to the pre-concentration of intracellular phosphate in these organisms. The results indicate that foraminifera may play a key and previously overlooked role in the global phosphorus cycle.

1 Introduction

Phosphorus (P) is essential for all living organisms. It is a fundamental component of nucleic acids (DNA, RNA), phospholipids, phosphoproteins, and in the transmission of chemical energy through the utilization of energy-rich phosphate bonds (Lehninger et al., 1993; Lipmann, 2006; Paytan and McLaughlin, 2007). The main sources of P to the oceans are continental weathering and atmospheric deposition through aerosols, volcanic ash, and mineral dust (Benitez-Nelson, 2000; Wallmann, 2010). The main oceanic P-sink is burial in marine sediments as authigenic minerals such as finely dispersed carbonate fluorapatite (CFA) or in the form of organic P (P_{org})

(Froelich et al., 1988; Delaney, 1998; Ingall, 2010; Wallmann, 2010). The process of authigenic precipitation of P-bearing minerals, largely in the form of CFA, is called phosphogenesis (Filippelli and Delaney, 1992; Filippelli, 2011). Another less quantified sink for oceanic P is microbially-mediated phosphogenesis in the upper few cm of the sediments within oxygen minimum zones (OMZs), leading to the formation of phosphorite precursors (Paytan and McLaughlin, 2007). Phosphorites are defined as phosphatic rocks with a P content of 10-20% (Blatt et al., 1996; Filippelli, 2011).

Intracellular total dissolved inorganic phosphate (DIP) concentrations ($[DIP]_i$, where i denotes an intracellular reservoir) can vary depending on the cell function. For example, $[DIP]_i$ can range between 0.5 and 0.8 mM in human erythrocytes and between 10 to 50 mM in the bacterium *Streptococcus bovis* JB1 (Bevington et al., 1986; Bond and Russell, 1998). Polyphosphates (P_{poly}) are an additional intracellular P-pool in a wide range of organisms, from prokaryotes to mammals, and can have various biological functions (Kornberg et al., 1999). Yeast cells store P_{poly} in vacuoles to remobilize DIP in times of DIP starvation (Thomas and O'Shea, 2005). Large sulfur oxidizing bacteria, such as *Beggiatoa sp.*, are also able to store P_{poly} granules intracellularly. These bacteria synthesize P_{poly} under oxic or nitrogenous conditions, whereupon it can be later hydrolysed and remobilized under anoxic conditions to provide energy (Sannigrahi and Ingall, 2005; Schulz and Schulz, 2005). This process can have a strong feedback on the benthic fluxes of DIP to the water column and the removal of DIP by phosphogenesis (Ingall and Jahnke, 1994; Goldhammer et al., 2010; Lomnitz et al., 2016; Dale et al., 2016a). Other studies have, however, shown that DIP release from microbial P_{poly} hydrolysis does not necessarily mediate phosphogenesis (Sulu-Gambari et al., 2016).

In-situ benthic flux measurements and sediment analyses on the Peruvian margin showed that benthic DIP release from sediments at the upper boundary of the OMZ is closely balanced by P inputs, whereas sediments at the lower OMZ boundary act as a P-sink due to massive phosphorite crust formation (Lomnitz et al., 2016). Within the core of the Peruvian OMZ, benthic DIP release is higher than P-input, indicating an additional source of DIP within the sediments (Lomnitz et al., 2016). This source is likely an intracellular DIP-pool, stored within microbes: Sediments subjected to repeated freezing and thawing released large amounts of DIP to sediment pore waters, leading to the hypothesis that nitrate-storing bacteria and benthic foraminifera might be responsible for the hidden DIP pool (Lomnitz et al., 2016). Risgaard-Petersen et al. (2006) made a similar observation on nitrate (NO_3^-) extracted from centrifuged Swedish fjord sediments and speculated that the NO_3^- mainly originated from cell lysis of benthic foraminifera. Several benthic foraminiferal species store NO_3^- within their cells as an alternative electron acceptor in times of O_2 depletion (Risgaard-Petersen et al., 2006; Piña-Ochoa et al., 2010; Woehle et al., 2018; Glock et al., 2019). These foraminifera account for a substantial hidden NO_3^- pool within sediments of the Peruvian OMZ (Glock et al., 2013; Dale et al., 2016b), yet their internal DIP pool has received less attention. These diverse results highlight the need to improve our understanding of P cycling in marine sedimentary environments.

Here, we present measurements of intracellular DIP content for five different benthic foraminiferal species from the Peruvian OMZ. We further examine the correlation between intracellular DIP and the foraminiferal cell volume to extrapolate our findings to other species not investigated here. Observed foraminiferal abundances are used to estimate the total benthic foraminiferal DIP reservoir in the Peruvian OMZ. Results of our study reveal a large hidden DIP pool stored within

benthic foraminifera. We suggest that this DIP reservoir has a strong impact on benthic P-cycling and might initiate phosphogenesis and ultimately contribute to the formation of phosphorites.

2 Methods

2.1 Sampling of living foraminifera

Fifteen short sediment cores from the Peruvian OMZ were retrieved during RV Meteor cruise M137 (May 2017) using a video-guided multiple corer (MUC). The inner diameter of the coring tubes was 10 cm. Three additional push-cores (diameter 10 cm) were taken from sediment retrieved inside a benthic incubation chamber after measuring solutes fluxes at the seafloor for ca. 36 h (Table 1, fig.1). Dissolved O_2 was below detection limit (3 µM) inside the benthic flux chambers throughout the incubation at these three stations. Immediately after core retrieval, the supernatant water was carefully removed. The top three cm of the core were sliced at one cm intervals for the analyses of the intracellular nutrient content. The sediment core slices were immediately sieved through a 63-µm mesh using surface seawater. The 63 to 2,000 µm residue was collected in 60 ml polypropylene beakers. Living foraminiferal specimens were identified under the binocular microscope by their colored chamber filling, hence the presence of cytoplasm, as well as by their pseudopodial activity. The most relevant species for this study are shown in Figure 2. Taxonomic references are given in Appendix 1.

For the analyses of the living foraminiferal fauna, the top three cm of another core from the same MUC cast or BIGO chamber were collected as a single slice, or as three 1-cm slices that were analysed separately. If sediment was needed for other analyses, the top three cm were collected with a cut off 50 ml syringe. The sediment was transferred to PVC bottles, stained and preserved

106 with a solution of two grams of rose Bengal L^{-1} ethanol (Schönfeld, 2012). The foraminiferal
107 assemblages of these samples were analysed by applying standard protocols (Schönfeld et al.,
108 2013; Lübbers and Schönfeld, 2018). Selected calcareous species of the Peruvian foraminiferal
109 fauna retrieved during M137 were described by Erdem et al., (2019). In addition, we compared the
110 new assemblage data from M137 to assemblages that were retrieved during an earlier Meteor
111 cruise (M77-1; November 2008). The sampling procedure during M77-1 was documented in Glock
112 et al. (2013). The complete faunal census data from M137 surface samples are given in the
113 appendix (Tab. A1). The species assemblages from M77-1 samples are listed in detail in Glock et
114 al. (2013). Faunal references for the most important species considered in the present study are
115 given in Appendix 1. In summary, the following methods were applied to samples from M77:

116 - Determination of foraminiferal abundances
117 - Photo-documentation of phosphatized foraminifera (described below)

118 The following methods were applied to samples from M137:

119 - Determination of foraminiferal abundances
120 - Analyses of intracellular DIP and NO_3^- content (described below)
121 - Determination of foraminiferal biovolume (described below)

122 **2.2 Cleaning, extraction and analytical procedure**

123 Depending on the size of the foraminiferal species and, thus, the amount of extracted DIP from a
124 single specimen, 8 to 138 specimens were picked for each replicate into a clean petri-dish with
125 nitrate- and phosphate-free artificial seawater prepared from Red Sea salt and gently cleaned with
126 a brush. They were then rinsed three times with artificial seawater and transferred into a pre-
127 cleaned polyethylene-beaker filled with 3 mL of reverse osmosis water (ROW) with a conductivity

of 0.055 µS cm^{-1}. Of the 25 samples containing living foraminifera, 16 were crushed (i.e. broken into small shards) within the beaker using a pre-cleaned polyethylene pipette tip. For every sample batch, a blank was carried through the same procedure without foraminiferal specimens (9 blanks in total). Three additional samples were taken consisting of dead, empty foraminiferal tests without any visible cytoplasm. These negative controls were crushed as well. All samples were frozen at – 20°C for at least two hours, and thawed afterwards. Freeze-thaw injuries damage plasma membranes and increase their permeability (Burke et al., 1976; Steponkus, 1984). This procedure was repeated three times. Subsequently, samples were filtered through sterile 0.2 µm cellulose-acetate filters. The influence of the filter size was not tested in detail and we cannot exclude possible contamination by organic or inorganic colloids. The filtered samples were analysed for NO_3^-+NO_2^- and total dissolved phosphate (DIP) on board using a QuAAtro autoanalyzer (SealAnalytical) and standard analytical methods (Grasshoff et al., 1999). NO_3^- was determined after subtracting NO_2^-. Detection limits based on the lowest calibration standards were 50 nM for NO_3^- and 35 nM for DIP. Analytical precision of NO_3^- and DIP determinations, based on repeated analysis of a certified seawater standard, was 2 % and 1 %, respectively. The analyzed sample volume was ~2.5 mL.

The procedural blanks showed an elevated concentration of 0.7 to 1.5 µmol/kg NO_3^- (1.0 ± 0.3 µmol/kg; 1sd; n = 9) but only lightly elevated concentrations of 0.05 to 0.11 µmol/kg DIP (0.06 ± 0.03 µmol/kg; 1sd; n = 9; sd = standard deviation). All specimen samples were blank-corrected with the procedural blank determined from the same batch on the same day. Surprisingly, the empty tests contained 17.9 (±9.3) % (1 sd; N = 3; absolute uncertainty) of NO_3^- and 4.7 (±1.6) % (1 sd; N = 3; absolute uncertainty), respectively, of the $NO_3^-$and DIP per biovolume unit measured in the living specimens of the same species and samples of the same batches.

151

152 **2.3 Biovolume determination**

153 Total foraminiferal cell volume of each species was estimated following Geslin et al. (2011) using
154 the best-resembling geometric shape (Tab. 2). We assumed that the internal test volume
155 corresponds to 75% of the total test volume and was completely filled with cytoplasm (Hannah et
156 al, 1994). The shell size parameters (length, width, and height) of each specimen were measured
157 using a Sentech™ STC-MC202USB-camera mounted on the ocular of a Leica™ M50 stereo
158 microscope. Photographs of each sample were taken before transfer into the PE-beaker filled with
159 ROW. The height of the specimens was required to estimate the volume of *Bolivina spissa* (flat
160 cone) and *Cassidulina limbata* (tri-axial ellipsoid) but was not determined for specimens that were
161 analyzed for the intracellular nutrient content. The height of *B. spissa* specimens was estimated by
162 measuring the mean height of the species (133 ± 7 µm; 151 N = 3). The height of *C. limbata*
163 specimens was estimated by correlating length (l) and height (h) determined on empty tests of this
164 species from the same samples ($h = 0.48 \cdot l - 28.9$; $R^2 = 0.73$; N = 10).

165 **2.4 Comparison of extraction methods (crushed vs uncrushed)**

166 For crushed samples (i.e. samples where foraminiferal tests were broken before analysis), the mean
167 intracellular NO_3^- concentration ($[NO_3^-]_i$) was 115 ± 19 mM (1 standard error of the mean (SEM);
168 n = 16) while the mean $[DIP]_i$ was 28 ± 3 mM (1 SEM; n = 16). The uncrushed samples had
169 significantly lower $[NO_3^-]_i$ (25 ± 8 mM; 1SEM; n = 8; P = 0.0003) but similar $[DIP]_i$ (21 ± 6 mM;
170 1SEM; n = 8; P = 0.29; two-sided heteroskedastic Student´s T-Test). This indicated that
171 intracellularly-stored nutrient was not extracted quantitatively in the uncrushed foraminiferal
172 specimens and that the DIP extraction was more efficient than the NO_3^- extraction. The extraction

was also more efficient for the smaller species when specimens were not crushed (Fig. 3), whereas *B. costata* showed the same $[NO_3^-]_i$ and $[DIP]_i$ for the crushed and the uncrushed treatment.

2.5 Photographs of phosphatized foraminifera

Photographs for documentation of the phosphatized foraminifera, shown in figure 4, were taken either with a MPX2050 CCD-camera from AOS™ coupled with a Navitar™ 6.5x zoom or with a Sentech™ STC-MC202USB-camera mounted on the ocular of a Leica™ M50 stereo microscope. The specimens were collected during M77-1 at 11°S off Peru between 640 and 928 m water depth at the sampling locations M77-1-565/MUC-60, M77-1-604/MUC-74 and M77-1-445/MUC-15. Foraminifera were picked from the surface interval (0-1 cm) of the sediment cores.

2.6 Calculation of benthic DIP stored in foraminifera

Using the composition of the benthic foraminiferal assemblages and the DIP_i for each species (Tab. 3), the benthic foraminiferal DIP pool in the sediment column ($\Sigma DIP_{i\ sed.}$ in mmol m^{-2}; depth intervals: 0-1 cm during M77 and 0-3 cm during M137) was calculated according to Eq1

Eq1: $$\Sigma DIP_{i\,sed} = \sum A_n \cdot DIP_{i\,n} \times 10^{-9}$$

where A_n is the abundance (living) of the foraminiferal species n in ind m^{-2} (ind. refers to individuals) and $DIP_{i\,n}$ is the mean intracellular DIP content of the species n in pmol ind^{-1}.The factor 10^{-9} was used to transform pmol to mmol.

The sedimentary intracellular [DIP] ($[DIP]_{i\ sed}$ in µmol L^{-1} of wet sediment) was calculated according to Eq2

Eq2: $$[DIP]_{i\,sed} = \sum PD_n \times DIP_{i\,n} \times 10^{-6}$$

where PD_n is the population density (living) of the foraminiferal species *n* in ind^{-1} L^{-1} of wet sediment and $DIP_{i\,n}$ is the mean intracellular DIP content of the species *n* in pmol ind^{-1}. The factor 10^{-6} was used to transform pmol to mmol.

Since DIP_i data were not available for every species, we considered the proportions of these species to the total biomass to scale-up the calculations to the total sediment according to Eq3 and Eq4:

Eq3: $$\Sigma DIP_{i\,sed\,tot} = \frac{\Sigma DIP_{i\,sed}}{A_{DIPi}/A_{tot}}$$

where $\Sigma TPO_{4i\,sed\,tot}$ is the total benthic foraminiferal DIP pool in the sediment column in mmol m^{-2}, A_{DIPi} is the abundance of foraminifera with known DIP_i in ind m^{-2}, and A_{tot} is the total foraminiferal abundance in ind m^{-2},

Eq4: $$[TDP]_{i\,sed\,tot} = \frac{[DIP]_{i\,sed}}{PD_{DIPi}/PD_{tot}}$$

$[TPO_4]_{i\,sed\,tot}$ is the total sedimentary intracellular [DIP] in µmol L^{-1} of wet sediment, PD_{DIPi} is the population density of foraminifera with known DIP_i in ind cm^{-3}, and PD_{tot} is the total foraminiferal population density in ind cm^{-3}.

Thus, if 90% of all foraminifera belong to species for which DIP_i were available, the total pool is 10% higher. This is the same approach as used by Glock et al. (2013). The percentages of species at each sampling location with known DIP_i are shown in Table 4. A detailed propagation of uncertainty was applied to estimate the error in the calculated DIP stored within foraminifera (for details see Appendix 2).

2.7 Phosphate metabolism in the genomes of foraminifera

Protein sequences of homolog proteins of lipid metabolism enzymes encoded in the foraminifera *Reticulomyxa filosa* (downloaded from the National Center for Biotechnology Information, NCBI, accession: GCA_000512085.1_Reti_assembly1.0, (Glöckner et al., 2014) and the transcriptome of the foraminifera *Globobulimina* spp. (NCBI accession: GGCD00000000.1) (Woehle et al., 2018) were identified using the emapper tool (Version 1.0.3, Parameter '-m diamond (--translate)', Huerta-Cepas et al., 2016) and obtained as KEGG Orthology annotations. The following protein types were identified to be associated with phosphate metabolism in the foraminifera datasets: PO_4^{3-} transporter (KO number: K08176), glycerol-3-phosphate dehydrogenases (K00006, K00111), glycerol kinases (K00864), manganese-dependent ADP-ribose/CDP-alcohol diphosphatases (K01517) and exopolyphosphatases (K01514, K01524).

3 Results

3.1 Intracellular DIP storage in foraminifera in relation to cell volume

We determined the intracellular DIP contents of *Bolivina costata*, *Bolivina interjuncta*, *Bolivina seminuda*, *C. limbata*, and *Valvulineria inflata* (Tab.5). One thousand foraminiferal specimens were used for the analyses. The mean intracellular DIP concentration ($[DIP]_i$) was 28 ± 3 mM (1SEM; n = 16). Individual DIP storage significantly increased with cell volume (Fig. 5; $R^2 = 0.97$; $p < 0.0001$). The correlation between cell volume and DIP storage (DIP_i in pmol ind^{-1}) (Fig. 5) can be described as a power function according to Eq5:

Eq5: $$\ln(DIP_i) = 0.82(\pm 0.03) \times \ln(V_{cell}) - 7.65\ (\pm 0.52)$$

or

Eq6: $$DIP_i = 4.76 \times 10^{-4} \times V_{cell}^{0.82(\pm 0.03)}$$

where V_{cell} is the cell volume in μm^3. Note that, due to the non-linearity of the power regressions the positive error of the constant $4.76x10^{-4}$ is different from the negative error ($+0.33x10^{-4}$ and $-0.19x10^{-4}$). Uncrushed samples of *B. costata* were also included in the power regression above, since the results were not different between the crushed and the uncrushed samples for this small species (Fig. 3).

3.2 Intracellular NO_3^- storage in foraminifera in relation to cell volume

Intracellular NO_3^- storage determined for *Bolivina costata*, *Bolivina interjuncta*, *Bolivina seminuda*, *C. limbata*, and *Valvulineria inflata* are listed in Tab. 5. The individual NO_3^- storage significantly increased with the cell volume (Fig. 6; $R^2 = 0.90$; $p < 0.0001$) and follows a power function :

Eq7: $$\ln(NO_{3\,i}^-) = 1.06(\pm 0.09) \times \ln(V_{cell}) - 10.29\ (\pm 1.43)$$

or

Eq8: $$NO_{3\,i}^- = 3.39 \times 10^{-5} \times V_{cell}^{1.06(\pm 0.09)}$$

where $NO_{3\,i}^-$ is the individual NO_3^- storage. Note that due to the non-linearity of the power regression the positive error of the constant $3.39x10^{-5}$ is different from the negative error ($+10.79x10^{-5}$ and $-2.59x10^{-5}$). As for DIP_i, uncrushed samples of *B. costata* were also included in the power regression since the results were not different between the crushed and the uncrushed samples (Fig. 3).

3.3 Total benthic DIP storage in sediments at the Peruvian OMZ

Mean biovolumes were determined for five additional foraminifera species from the Peruvian OMZ for which the intracellular nutrient content was not measured (Tab. 6). Their DIP_i was

calculated using Eq 5. The total benthic foraminiferal DIP pool in the upper 3 cm of sediment ($\Sigma DIP_{i\ sed\ tot.}$ in mmol m^{-2}) was then calculated according to Eq1 and Eq3, using the benthic foraminiferal assemblages in the Peruvian OMZ and the DIP_i for each species (Tab. 3). The total sedimentary intracellular [DIP] ($[DIP]_{i\ sed\ tot}$ in µmol L^{-1} of wet sediment) was calculated according to Eq2. and Eq4. The results from two sampling transects (11°S from RV Meteor cruise M77 and 12°S from cruise M137) across the Peruvian margin were compared (Tab. 7). Our results show that $\Sigma DIP_{i\ sed\ tot}$ reached up to 3.48 mmol m^{-2} (Tab. 7; Fig. 7) along the 12°S transect. $[DIP]_{i\ sed\ tot}$ in the top 3 cm of the sediments varied between 1 and 135 µmol L^{-1} of wet sediment. Along the 11°S transect, we only estimated the intracellular DIP concentration in the uppermost cm. Since most of the foraminifera in the Peruvian OMZ live in the top cm (Glock et al., 2013), it is reasonable to assume that the $[DIP]_{i\ sed\ tot}$ is up to three times higher in the first cm of the sediments along the 12°S transect (i.e. > 300 µmol l^{-1}) where the average in the top 3 cm was determined.

3.4 Enzymes involved in phosphate metabolism in foraminifera

The above results prompted us to investigate the genetic constituents of the foraminiferal DIP transport and metabolism. According to foraminiferal genomics databases, the genomes of *Reticulomyxa filosa* and *Globobulimina spp.* include genes encoding for a PO_4^{3-} transporter (e.g., the NCBI accessions: ETO28643.1, GGCD01019871.1). The function of these transporters in foraminifers likely enables active accumulation of DIP_i in the cell. With regard to enzymes of the phosphate metabolism pathway, both foraminifers encode homologs of glycerol-3-phosphate dehydrogenases (e.g., accessions: ETO22554.1, GGCD01001980.1), glycerol kinases (e.g., ETO32070.1, GGCD01026888.1), and manganese-dependent ADP-ribose/CDP-alcohol diphosphatase (e.g., ETO09651.1, GGCD01006605.1). These enzymes facilitate the production of sn-glycero-3-phosphate. In addition, we identified homologs of exopolyphosphatases (accessions:

277 ETO01067.1, GGCD01048558.1) that catalyze the hydrolysis of P_{poly} in eukaryotes. The
278 comparative genomics results thus support the notion that foraminifera possess the molecular
279 machinery for DIP-import and -metabolism, including the capacity for P_{poly} metabolism.

280 **4 Discussion**

281 Although the respiration of $NO_3^-{}_i$ by denitrifying foraminifera under anaerobic conditions is well-
282 documented (Risgaard-Petersen et al., 2006), the function of the high intracellular DIP_i enrichment
283 is unknown. The slope of the power function Eq.7 is close to 1 (Fig. 6), indicating a nearly linear
284 relationship of $NO_3^-{}_i$ with cell volume, which means that $NO_3^-{}_i$ is independent from the cell
285 volume. Contrastingly, the slope of eq. 5 (Fig. 5) indicates a nearly sublinear (slope close to 0.75)
286 relationship between DIP_i and the cell volume. Thus, larger foraminifera store a lower amount of
287 DIP_i normalized to the cell volume than smaller individuals, indicating that larger foraminifera
288 cannot efficiently sustain their demand for DIP_i. This might be related to local DIP oversaturation,
289 due to the high amount of DIP_i in larger cells (see discussion below regarding intracelular CFA
290 nucleation).

291 **4.1 Source and function of foraminiferal DIP_i**

292 Orthophosphate can be used for a wide range of biological functions including the synthesis of the
293 cellular energy carrier ATP (Lipmann, 2006). The average ATP concentration in the cytoplasm of
294 living benthic foraminifera has been shown to be ~0.8 mM (Bernhard, 1992). The DIP_i that we
295 measured may therefore partly originate from hydrolysed ATP extracted from the foraminifera,
296 but the latter is likely to be a minor component of the measured $[DIP]_i$. A DIP_i source from the
297 remineralization of organic matter by respiration or denitrification of the foraminifers can also be
298 excluded. This is supported by the denitrification and respiration rates published by Glock et al.

(2019) and a stoichiometry of 1 mole of PO_4^{3-} released during the denitrification of 104 moles of NO_3^- or the respiration 150 moles of O_2. The largest species in our study, *V. inflata*, would need 120 days to accumulate its DIP_i pool by denitrification and 450 days by O_2 respiration. The smallest species, *B. costata*, would require 163 days (denitrification) and 20 days (O_2 respiration). Other sources and mechanisms of DIP_i storage include the synthesis of P_{poly}, compounds that are present in every living cell (Kornberg et al., 1999) as well as the synthesis of phospholipids, constituents of the foraminifera plasma membrane (Langer and Bell, 1995). A precursor of all biological membrane phospholipids is sn-glycero-3-phosphate (Raetz, 1978). Foraminifera continuously change their surface to volume ratio by extrusion and intrusion of their pseudopodial network and by the inclusion of vacuoles within their cytoplasm. Thus, cellular membranes have to be continuously synthesized and broken down and the elevated intracellular DIP levels could serve as a reservoir for this process.

The speciation of DIP_i stored within the foraminiferal cells is unknown. Previous studies focused on fossil foraminiferal tests and reported that P is mainly located within Fe- and Mn-rich coatings rather than the carbonate matrix (Sherwood et al., 1987). We can exclude coatings as a source of the DIP_i extracted from living foraminifera since diagenetic overgrowth on tests is generally absent in Recent samples from the Peruvian OMZ (Glock et al., 2012). Furthermore, foraminifera discriminate against P during synthesis of tests (Palmer, 1985; Sherwood et al., 1987; Boyle, 2006). Thus, partial dissolution of the calcitic foraminiferal tests can be excluded as a source for the extracted DIP. In addition, the intracellular storage of P_{poly} has been documented for a wide range of organisms, including microorganisms, animals and plants (Kulaev and Kulakovskaya, 2000).

Cells are usually stained with OsO_4, prior to transmission electron microscopic (TEM) examination, to assure a good image contrast, since OsO_4 is electron-rich and, thus, the electron beam will not transmit through the stained regions (Palade, 1952). Most foraminiferal species have cell organelles of an unknown function inside their cytoplasm that appear as "electron-dense bodies" in TEM images, (Nomaki et al., 2016; Koho et al., 2018; LeKieffre et al., 2018). Similar electron-dense bodies have been observed in the green algae *Cosmarium* sp. and a parallel emergence of P_{poly} within their cells has led to the hypothesis that these granules are compact P_{poly} aggregates (Elgavish et al., 1980). These P_{poly} aggregates are stored together with calcium within acidocalcisomes (Elgavish et al., 1980). Acidocalcisomes are the only organelles present in both prokaryotic and eukaryotic organisms (Docampo et al., 2005). They have various functions, including storage of cations and phosphorus, polyphosphate metabolism, calcium homeostasis, maintenance of intracellular pH homeostasis and osmoregulation. The formation of P_{poly} within acidocalcisomes inhibits the intracellular precipitation of apatite (Kulakovskaya, 2014). The electron-dense bodies have also been observed in the pseudopodial network of some foraminifera (Travis and Bowser, 1991). It remains to be shown whether some of the electron-dense bodies observed in foraminifera are related to phospholipid precursors, P_{poly} or acidocalcisomes. Our findings on DIP metabolism in the genomes of foraminifera indicate the existence of enzymes for DIP import and metabolism, the capacity for a P_{poly} metabolism and the production of sn-glycero-3-phosphate, covering the metabolic pathways discussed above.

4.2 The role of foraminifers in benthic P-cycling and phosphogenesis

If P_{poly} is synthesized to prevent intracellular apatite formation, it may be released into the extracellular medium (i.e. the ambient porewater) after cell death and hydrolyzed by phosphatases. We speculate that *post-mortem* phosphogenesis might be initiated by the consequent local

344 oversaturation, as suggested for other microorganisms (Schulz and Schulz, 2005; Kulakovskaya,
345 2014).

346 Incubations using the radiotracer ^{45}Ca revealed that the planktic foraminifer *Globigerinoides*
347 *sacculifer* has a dissolved intracellular calcium pool of ~80 mM (Anderson and Faber, 1984),
348 which can even be higher in the benthic species *Amphestegina lobifera* (Erez, 2003). Our
349 experiments revealed that foraminifers from the Peruvian OMZ have an average intracellular DIP
350 pool of 28±3 mM. Several experiments have revealed that the precipitation of CFA can occur
351 under different seawater conditions when Ca and DIP concentrations are one to three orders-of-
352 magnitude lower (Gulbrandsen et al., 1984; Van Cappellen and Berner, 1991; Gunnars et al.,
353 2004). The time required for CFA to form in these experiments varied from several hours to several
354 years. It is difficult to predict the formation of different apatite phases under seawater conditions,
355 since many factors such as pH, Mg^{2+}, F^- and dissolved organic compound concentrations affect
356 the kinetics of apatite precipitation (Van Cappelen and Berner, 1991 and references therein). One
357 of the main factors known to kinetically hamper marine CFA precipitation is the presence of Mg^{2+}.
358 Furthermore, the formation of CFA under seawater conditions most likely proceeds via a precursor
359 pathway, involving octacalcium phosphate (OCP) rather than direct nucleation (Gunnars et al.,
360 2004). The formation of OCP appears to be inhibited under elevated Mg-concentrations and the
361 precipitation of OCP provides a kinetic boundary for the formation of apatite in natural seawater
362 (Gunnars et al., 2004). In addition, previous studies showed that calcite is the preferred substrate
363 for CFA precipitation under marine conditions (Lucas and Prévôt, 1985) and hydroxyapatite can
364 grow directly on calcite seed crystals even under a low degree of supersaturation and possibly
365 without the formation of precursor phases (Koutsoukos and Nancollas, 1981). Most calcitic
366 foraminiferal species (except milliolids) discriminate against Mg^{2+} incorporation into their test

367 calcite, and it has been suggested that they actively remove Mg^{2+} from their seawater vacuoles
368 (Erez, 2003; Bentov and Erez, 2006; de Nooijer et al., 2009). Thus, given that (i) the intracellular
369 Ca^{2+} and DIP concentrations are elevated by several orders of magnitude while Mg^{2+} is likely
370 depleted compared to the surrounding pore water, and (ii) that the calcite tests provide a preferred
371 substrate for CFA precipitation, the intratestular microenvironment *post mortem* may be optimum
372 for the precipitation of CFA.

373 The high DIP_i enrichment in benthic foraminifera, in combination with their high abundance, in
374 sediments from the Peruvian OMZ, underlines their possible relevance for benthic P-cycling. In
375 some locations, $\Sigma DIP_{i\ sed\ tot}$ was >3 mmol m^{-2} and the $[DIP]_{i\ sed\ tot}$ within the upper cm of the
376 sediment was >100 µmol L^{-1} (Tab. 7). This is the same order-of-magnitude as the [DIP] released
377 into the pore waters from freeze-thawed sediments from the Peruvian OMZ, possibly indicating
378 that a major part of the released DIP was stored in benthic foraminifera (Lomnitz et al., 2016). The
379 imbalance of benthic DIP fluxes and P inputs in sediments in the centre of the Peruvian OMZ may
380 be explained by a hidden (i.e. not yet specified) sedimentary DIP reservoir (Lomnitz et al., 2016).
381 Benthic DIP fluxes off Peru vary between 0.1 and 2.0 mmol m^{-2} day^{-1}, which is far higher than the
382 average global flux in pelagic sediments of 0.02 mmol m^{-2} day^{-1} (Wallmann, 2010; Noffke et al.,
383 2012; Lomnitz et al., 2016). The turnover time of the $\Sigma DIP_{i\ sed\ tot}$ pool can be as little as a few days
384 off Peru, compared to more than one year if the pelagic mean flux is assumed. Thus, the
385 foraminiferal DIP pool constitutes an important mobile reservoir on the Peruvian margin.

386 The highest foraminiferal DIP reservoir was observed between 400 and 500 m water depth at 12°S.
387 Negative benthic DIP fluxes at these depths indicate that the sediments are a P-sink and a site for
388 ongoing active phosphogenesis and phosphorite formation (Lomnitz et al., 2016). Dating of
389 phosphorite nodules from the Peruvian margin by uranium-series methods revealed that

390 contemporary phosphorite formation is ongoing (Veeh et al., 1973). We propose that the
391 intracellular phosphate reservoir in benthic foraminifera triggers phosphogenesis and facilitates
392 phosphorite formation under favourable environmental conditions, e.g. low sedimentation rates or
393 strong erosion (Manheim et al., 1975). Several studies have emphasized the role of microbiota in
394 phosphogenesis in environments where sediment chemistry is not kinetically favourable (Schulz
395 and Schulz, 2005; Diaz et al., 2008; Goldhammer et al., 2010). For instance, intracellular
396 assimilation of P by bacteria might facilitate phosphogenesis because phosphorites on the eastern
397 Australian continental margin contain bacteria that have been phosphatized (O'Brien et al., 1981).
398 The phosphogenesis likely occurred rapidly *post-mortem* since the shape of the bacteria was well
399 preserved. Similarly, several studies documented numerous granular phosphorites containing
400 phosphorite grains nucleated in or around foraminiferal tests (Slansky, 1986; Lamboy, 1993). An
401 additional study on the upper continental slope of the Peruvian margin reported high inorganic P
402 content in phosphorites within foraminifera that were all Holocene benthic species (Manheim et
403 al., 1975). These benthic foraminiferal phosphorite pellets showed transitional stages from plain
404 foraminiferal tests to featureless phosphorite grains with the original shape of a foraminifer. It was
405 suggested that phosphogenesis started within the foraminiferal test and had no direct link to the
406 carbonate of the original test which started to dissolve after the initial authigenic phase formed
407 (Lamboy, 1993). Similar phosphatized foraminifera were frequent in our samples (Fig. 4) and also
408 larger phosphorite nodules from the Peruvian OMZ were characterized by numerous encrusted
409 foraminifera (Resig and Glenn, 1997).

410 This evidence supports our hypothesis that DIP stored within benthic foraminifera plays a role in
411 phosphogenesis and the formation of recent phosphorites at the lower boundary of the Peruvian
412 OMZ. Nevertheless, phosphorite formation also takes place at the upper OMZ boundary (~150 m)

(Resig and Glenn, 1997). Both environments are strongly erosive due to vigorous bottom currents at the upper boundary (Resig and Glenn, 1997) and internal waves at the lower boundary (Mosch et al., 2012; Erdem et al., 2016). Whereas P_{poly} enrichments in sulphur oxidizing bacterial mats and possibly foraminifera facilitate phosphogenesis at the upper OMZ boundary, bacterial mats are absent at the lower boundary (Mosch et al., 2012; Lomnitz et al., 2016). Net fluxes of 0.07 mmol mm^{-2} P d^{-1} into the sediment have been reported at a station from 403 m depth at 12°S (Lomnitz et al., 2016) where phosphorite formation is ongoing and phosphorite deposits are found. We found a mean $\Sigma DIP_{i\ sed\ tot}$ of 1.81 ± 1.55 (1sd) mmol m^{-2} between 400 and 500 m depth. This result can be used as a rough estimate of the contribution of benthic foraminifers to the benthic DIP-burial, considering their mortality and lifespan. A study on staining with the vital dye cell-tracker green revealed that about 50% of benthic foraminifera containing cytoplasm might be dead (Bernhard et al., 2006). The lifespan of benthic foraminifers is species-dependant and can vary between two weeks and >1 year (Boltovskoy and Wright, 1976). If we consider this range, we can assume that 50% of the $\Sigma DIP_{i\ sed\ tot}$ is released within 14 to 365 days following the death of foraminifera and channeled into phosphogenesis. This leads to a maximum burial of 0.002 to 0.064 mmol DIP m^{-2} day^{-1} by phosphogenesis, initiated *post-mortem* in foraminifers, which is equal to 3 to 91% of the total net DIP flux.

In a previous model to explain the presence of phosphatized microbial mats within phosphatic rocks, it was suggested that phosphogenesis is initiated by the rapid burial of living microbes during early diagenesis (Reimers et al., 1990). These authors hypothesized that the associated DIP release from the sediments, originating from the remineralization of P-accumulating organisms, can be capped by the DIP accumulation of a new generation of living, P-accumulating microbes within the top centimeters of the sediments, leading to hotspots of sedimentary P-accumulation.

However, such a mechanism requires repeated cycles of catastrophic burial events by displacement of sand or deposition of organic mud followed by winnowing events to re-expose the phosphatized microbes (Föllmi, 1990; Föllmi et al., 2005). Whether the structures that have been described as phosphatized microbial mats are fossilized microbes or authigenic phosphate minerals that coincidentally have the shape of microbial mats is still under debate (Van Cappellen and Berner, 1991; Föllmi et al., 2005). Nevertheless, a similar "capping mechanism" can be assumed for DIP-accumulating foraminifera, preventing the sedimentary DIP release from remineralization or dissolution of phosphatic minerals. Thus, foraminifera may play a key role in the P-cycling within the Peruvian OMZ and possibly other habitats with similarly high foraminiferal abundance.

5 Acknowledgements

The scientific party and crew on R/V Meteor cruise M137 and chief scientist Stefan Sommer are gratefully acknowledged for their support at sea and assistance with sediment coring. We thank Bettina Domeyer for performing the nutrient analyses. N.G. would also like to thank Anton Eisenhauer, Volker Liebetrau and Hidetaka Nomaki for fruitful scientific discussions. Funding was provided by the Deutsche Forschungsgemeinschaft (DFG) through the SFB 754 "Climate–Biogeochemistry Interactions in the Tropical Ocean". Finally, we would like to acknowledge four anonymous reviewers and associate editor Alfonso Mucci, whose comments significantly improved our manuscript.

6 Author Contributions

N.G., D.R., and A.D. developed the cleaning and extraction methods. D.R. and N.G. performed the cleaning of foraminiferal specimens and extraction of nutrients. C.W. performed the genomics database analysis. J.S. did the analyses of the foraminiferal assemblages. N.G., D.R., A.-S.R.,

458 T.W., J.W. and T.D. were all involved in the sampling procedure. N.G., A.S.R. and T.D. planned
459 the expedition and experiments. All authors contributed writing this manuscript.

460 **References:**

461 Anderson O. R. and Faber W. W. (1984) An estimation of calcium carbonate deposition rate in a
462 planktonic foraminifer Globigerinoides sacculifer using 45 Ca as a tracer; a recommended
463 procedure for improved accuracy. *J. Foraminifer. Res.* **14**, 303–308.

464 Benitez-Nelson C. R. (2000) The biogeochemical cycling of phosphorus in marine systems.
465 *Earth-Science Rev.* **51**, 109–135.

466 Bentov S. and Erez J. (2006) Impact of biomineralization processes on the Mg content of
467 foraminiferal shells: A biological perspective. *Geochemistry, Geophys. Geosystems* **7**.

468 Bernhard J. M. (1992) Benthic foraminiferal distribution and biomass related to pore-water
469 oxygen content: central California continental slope and rise. *Deep Sea Res. Part A,*
470 *Oceanogr. Res. Pap.* **39**, 585–605.

471 Bernhard J. M., Ostermann D. R., Williams D. S. and Blanks J. K. (2006) Comparison of two
472 methods to identify live benthic foraminifera: A test between Rose Bengal and CellTracker
473 Green with implications for stable isotope paleoreconstructions. *Paleoceanography* **21**.

474 Bevington A., Mundy K. I., Yates A. J., Kanis J. A., Russell R. G., Taylor D. J., Rajagopalan B.
475 and Radda G. K. (1986) A study of intracellular orthophosphate concentration in human
476 muscle and erythrocytes by 31P nuclear magnetic resonance spectroscopy and selective
477 chemical assay. *Clin. Sci. (Lond).* **71**, 729–35.

478 Blatt H., Tracy R. J. and Ehlers E. G. (1996) *Petrology : igneous, sedimentary, and*
479 *metamorphic.*, W.H. Freeman.

480 Boltovskoy E. and Wright R. (1976) Ecology. In *Recent Foraminifera* Springer Netherlands,
481 Dordrecht. pp. 223–274.

482 Bond D. R. and Russell J. B. (1998) Relationship between intracellular phosphate, proton motive
483 force, and rate of nongrowth energy dissipation (Energy spilling) in Streptococcus bovis
484 JB1. *Appl. Environ. Microbiol.* **64**, 976–981.

485 Boyle E. A. (2006) A Direct Proxy for Oceanic Phosphorus? *Science (80-.).* **312**, 1758 LP –
486 1759.

487 Burke M. J., Gusta L. V, Quamme H. A., Weiser C. J. and Li P. H. (1976) Freezing and Injury in
488 Plants. *Annu. Rev. Plant Physiol.* **27**, 507–528.

489 Van Cappellen P. and Berner R. A. (1991) Fluorapatite crystal growth from modified seawater
490 solutions. *Geochim. Cosmochim. Acta* **55**, 1219–1234.

491 Dale A. W., Boyle R. A., Lenton T. M., Ingall E. D. and Wallmann K. (2016a) A model for
492 microbial phosphorus cycling in bioturbated marine sediments: Significance for phosphorus
493 burial in the early Paleozoic. *Geochim. Cosmochim. Acta* **189**, 251–268.

494 Dale A. W., Sommer S., Lomnitz U., Bourbonnais A. and Wallmann K. (2016b) Biological
495 nitrate transport in sediments on the Peruvian margin mitigates benthic sulfide emissions
496 and drives pelagic N loss during stagnation events. *Deep Sea Res. Part I Oceanogr. Res.*
497 *Pap.* **112**, 123–136.

498 Delaney M. L. (1998) Phosphorus accumulation in marine sediments and the oceanic phosphorus
499 cycle. *Global Biogeochem. Cycles* **12**, 563–572.

500 Diaz J., Ingall E., Benitez-Nelson C., Paterson D., De Jonge M. D., McNulty I. and Brandes J. A.
501 (2008) Marine polyphosphate: A key player in geologic phosphorus sequestration. *Science*
502 *(80-.).* **320**, 652–655.

503 Docampo R., de Souza W., Miranda K., Rohloff P. and Moreno S. N. J. (2005)
504 Acidocalcisomes ? conserved from bacteria to man. *Nat. Rev. Microbiol.* **3**, 251–261.

505 Elgavish A., Elgavish G. A. and Halmann M. (1980) Intracellular phosphorus pools in intact
506 algal cells. *FEBS Lett.* **117**, 137–142.

507 Erdem Z., Schönfeld J., Glock N., Dengler M., Mosch T., Sommer S., Elger J. and Eisenhauer A.
508 (2016) Peruvian sediments as recorders of an evolving hiatus for the last 22 thousand years.
509 *Quat. Sci. Rev.* **137**, 1–14.

510 Erdem Z., Schönfeld J., Rathburn A. E., Pérez M.-E., Cardich J. and Glock N. (2019) Bottom-
511 water deoxygenation at the Peruvian Margin during the last deglaciation recorded by
512 benthic foraminifera. *Biogeosciences Discuss.* **2019**, 1–37.

513 Erez J. (2003) The Source of Ions for Biomineralization in Foraminifera and Their Implications
514 for Paleoceanographic Proxies. *Rev. Mineral. Geochemistry* **54**, 115–149.

515 Filippelli G. M. (2011) Phosphate rock formation and marine phosphorus geochemistry: The
516 deep time perspective. *Chemosphere* **84**, 759–766.

517 Filippelli G. M. and Delaney M. L. (1992) Similar phosphorus fluxes in ancient phosphorite
518 deposits and a modern phosphogenic environment. *Geology* **20**, 709–712.

519 Föllmi K. B. (1990) Condensation and phosphogenesis: example of the Helvetic mid-Cretaceous
520 (northern Tethyan margin). *Geol. Soc. London, Spec. Publ.* **52**, 237 LP – 252.

521 Föllmi K. B., Badertscher C., de Kaenel E., Stille P., John C. M., Adatte T. and Steinmann P.
522 (2005) Phosphogenesis and organic-carbon preservation in the Miocene Monterey
523 Formation at Naples Beach, California—The Monterey hypothesis revisited. *GSA Bull.* **117**,
524 589–619.

525 Froelich P. N., Arthur M. A., Burnett W. C., Deakin M., Hensley V., Jahnke R., Kaul L., Kim K.
526 H., Roe K., Soutar A. and Vathakanon C. (1988) Early diagenesis of organic matter in Peru
527 continental margin sediments: Phosphorite precipitation. *Mar. Geol.* **80**, 309–343.

528 Geslin E., Risgaard-petersen N., Lombard F., Metzger E., Langlet D. and Jorissen F. (2011)
529 Oxygen respiration rates of benthic foraminifera as measured with oxygen microsensors. *J.*
530 *Exp. Mar. Bio. Ecol.* **396**, 108–114.

531 Glock N., Eisenhauer A., Liebetrau V., Wiedenbeck M., Hensen C. and Nehrke G. (2012) EMP

and SIMS studies on Mn/Ca and Fe/Ca systematics in benthic foraminifera from the Peruvian OMZ: A contribution to the identification of potential redox proxies and the impact of cleaning protocols. *Biogeosciences* **9**.

Glock N., Roy A.-S., Romero D., Wein T., Weissenbach J., Revsbech N. P., Høgslund S., Clemens D., Sommer S. and Dagan T. (2019) Metabolic preference of nitrate over oxygen as an electron acceptor in foraminifera from the Peruvian oxygen minimum zone. *Proc. Natl. Acad. Sci.* **116**, 2860–2865.

Glock N., Schönfeld J., Eisenhauer A., Hensen C., Mallon J. and Sommer S. (2013) The role of benthic foraminifera in the benthic nitrogen cycle of the Peruvian oxygen minimum zone. *Biogeosciences* **10**, 4767–4783.

Glöckner G., Hülsmann N., Schleicher M., Noegel A. A., Eichinger L., Gallinger C., Pawlowski J., Sierra R., Euteneuer U., Pillet L., Moustafa A., Platzer M., Groth M., Szafranski K. and Schliwa M. (2014) The genome of the foraminiferan Reticulomyxa filosa. *Curr. Biol.* **24**, 11–18.

Goldhammer T., Brüchert V., Ferdelman T. G. and Zabel M. (2010) Microbial sequestration of phosphorus in anoxic upwelling sediments. *Nat. Geosci.* **3**, 557–561.

Grasshoff K., Kremlingl K. and Ehrhardt M. (1999) *Methods of Seawater Analysis*., Wiley, Weinheim.

Gulbrandsen R. A., Roberson C. E. and Neil S. T. (1984) Time and the crystallization of apatite in seawater. *Geochim. Cosmochim. Acta* **48**, 213–218.

Gunnars A., Blomqvist S. and Martinsson C. (2004) Inorganic formation of apatite in brackish seawater from the Baltic Sea : an experimental approach. **91**, 15–26.

Huerta-Cepas J., Forslund K., Szklarczyk D., Jensen L. J., Mering C. von and Bork P. (2016) Fast genome-wide functional annotation through orthology assignment by eggNOG-mapper. *bioRxiv*, 076331.

Ingall E. D. (2010) Phosphorus burial. *Nat. Geosci.* **3**, 521–522.

Ingall E. and Jahnke R. (1994) Evidence for enhanced phosphorus regeneration from marine sediments overlain by oxygen depleted waters. *Geochim. Cosmochim. Acta* **58**, 2571–2575.

Koho K. A., LeKieffre C., Nomaki H., Salonen I., Geslin E., Mabilleau G., Søgaard Jensen L. H. and Reichart G. J. (2018) Changes in ultrastructural features of the foraminifera Ammonia spp. in response to anoxic conditions: Field and laboratory observations. *Mar. Micropaleontol.* **138**, 72–82.

Kornberg A., Rao N. N. and Ault-riché D. (1999) Inorganic Polyphosphate: A Molecule of Many Functions. *Annu. Rev. Biochem.* **68**, 89–125.

Koutsoukos P. G. and Nancollas G. H. (1981) Crystal growth of calcium phosphates - epitaxial considerations. *J. Cryst. Growth* **53**, 10–19.

Kulaev I. and Kulakovskaya T. (2000) P Olyphosphate and P Hosphate P Ump. *Energy Source*, 709–734.

Kulakovskaya T. (2014) Phosphorus storage in Microorganisms: Diversity and Evolutionary Insight. *Biochem. Physiol. Open Access* **04**, 1–4.

Lamboy M. (1993) Phosphatization of calcium carbonate in phosphorites: microstructure and importance. *Sedimentology* **40**, 53–62.

Langer M. R. and Bell C. J. (1995) Toxic foraminifera: Innocent until proven guilty. *Mar. Micropaleontol.* **24**, 205–214.

Lehninger A. L., Nelson D. L. and Cox M. M. (1993) *Principles of Biochemistry*. 2nd ed., Worth Publishers, 33 Irving Place, New York, NY.

LeKieffre C., Bernhard J. M., Mabilleau G., Filipsson H. L., Meibom A. and Geslin E. (2018) An overview of cellular ultrastructure in benthic foraminifera: New observations of rotalid species in the context of existing literature. *Mar. Micropaleontol.* **138**, 12–32.

Lipmann F. (2006) Metabolic Generation and Utilization of Phosphate Bond Energy. In Wiley-Blackwell. pp. 99–162.

Lomnitz U., Sommer S., Dale A. W., Löscher C. R., Noffke A., Wallmann K. and Hensen C. (2016) Benthic phosphorus cycling in the Peruvian oxygen minimum zone. *Biogeosciences* **13**, 1367–1386.

Lübbers J. and Schönfeld J. (2018) Recent saltmarsh foraminiferal assemblages from Iceland. *Estuar. Coast. Shelf Sci.* **200**, 380–394.

Lucas J. and Prévôt L. (1985) The synthesis of apatite by bacterial activity : mechanism. *Sci. Géologiques. Mémoire Mech.* **77**, 83–92.

Manheim F., Rowe G. T. and Jipa D. (1975) Marine phosphorite formation off Peru. *J. Sediment. Res.* **45**, 243–251.

Mosch T., Sommer S., Dengler M., Noffke A., Bohlen L., Pfannkuche O., Liebetrau V. and Wallmann K. (2012) Factors influencing the distribution of epibenthic megafauna across the Peruvian oxygen minimum zone. *Deep Sea Res. Part I Oceanogr. Res. Pap.* **68**, 123–135.

Noffke A., Hensen C., Sommer S., Scholz F., Bohlen L., Mosch T., Graco M. and Wallmann K. (2012) Benthic iron and phosphorus fluxes across the Peruvian oxygen minimum zone. *Limnol. Oceanogr.* **57**, 851–867.

Nomaki H., Bernhard J. M., Ishida A., Tsuchiya M., Uematsu K., Tame A., Kitahashi T., Takahata N., Sano Y. and Toyofuku T. (2016) Intracellular isotope localization in Ammonia sp. (Foraminifera) of oxygen-depleted environments: Results of nitrate and sulfate labeling experiments. *Front. Microbiol.* **7**, 1–12.

de Nooijer L. J., Toyofuku T. and Kitazato H. (2009) Foraminifera promote calcification by elevating their intracellular pH. *Proc. Natl. Acad. Sci.* **106**, 15374 LP – 15378.

O'Brien G. W., Harris J. R., Milnes A. R. and Veeh H. H. (1981) Bacterial origin of East Australian continental margin phosphorites. *Nature* **294**, 442–444.

Palade G. E. (1952) A STUDY OF FIXATION FOR ELECTRON MICROSCOPY . *J. Exp. Med.* **95**, 285–298.

608 Palmer M. R. (1985) Rare earth elements in foraminifera tests. *Earth Planet. Sci. Lett.* **73**, 285–
609 298.

610 Paytan A. and McLaughlin K. (2007) The Oceanic Phosphorus Cycle. *Chem. Rev.* **107**, 563–576.

611 Piña-Ochoa E., Høgslund S., Geslin E., Cedhagen T., Revsbech N. P., Nielsen L. P., Schweizer
612 M., Jorissen F., Rysgaard S. and Risgaard-Petersen N. (2010) Widespread occurrence of
613 nitrate storage and denitrification among Foraminifera and Gromiida. *Proc. Natl. Acad. Sci.*
614 **107**, 1148–1153.

615 Raetz C. R. (1978) Enzymology, genetics, and regulation of membrane phospholipid synthesis in
616 Escherichia coli. *Microbiol Rev* **42**, 614–659.

617 Reimers C. E., Kastner M. and Garrison R. E. (1990) The role of bacterial mats in phosphate
618 mineralization with particular reference to the Monterey Formation. *Phosphate Depos.*
619 *World* **3**, 300–311.

620 Resig J. M. and Glenn C. R. (1997) Foraminifera encrusting phosphoritic hardgrounds of the
621 Peruvian upwelling zone; taxonomy, geochemistry, and distribution. *J. Foraminifer. Res.*
622 **27**, 133–150.

623 Risgaard-Petersen N., Langezaal A. M., Ingvardsen S., Schmid M. C., Jetten M. S. M., Op Den
624 Camp H. J. M., Derksen J. W. M., Piña-Ochoa E., Eriksson S. P., Nielsen L. P., Revsbech
625 N. P., Cedhagen T. and Van Der Zwaan G. J. (2006) Evidence for complete denitrification
626 in a benthic foraminifer. *Nature* **443**, 93–96.

627 Sannigrahi P. and Ingall E. (2005) Polyphosphates as a source of enhanced P fluxes in marine
628 sediments overlain by anoxic waters: Evidence from 31P NMR. *Geochem. Trans.* **6**, 52.

629 Schönfeld J. (2012) History and development of methods in Recent benthic foraminiferal studies.
630 *J. Micropalaeontology* **31**, 53–72.

631 Schönfeld J., Golikova E., Korsun S. and Spezzaferri S. (2013) The Helgoland Experiment –
632 assessing the influence of methodologies on Recent benthic foraminiferal assemblage
633 composition. *J. Micropalaeontology* **32**, 161–182.

634 Schulz H. N. and Schulz H. D. (2005) Large sulfur bacteria and the formation of phosphorite.
635 *Science* **307**, 416–8.

636 Sherwood B. A., Sager S. L. and Holland H. D. (1987) Phosphorus in foraminiferal sediments
637 from North Atlantic Ridge cores and in pure limestones. *Geochim. Cosmochim. Acta* **51**,
638 1861–1866.

639 Slansky M. (1986) *Geology of sedimentary phosphates*.,

640 Steponkus P. L. (1984) Injury and Cold Acclimation. *Annu. Rev. Plant Physiol.* **35**, 543–584.

641 Sulu-Gambari F., Seitaj D., Meysman F. J. R., Schauer R., Polerecky L. and Slomp C. P. (2016)
642 Cable Bacteria Control Iron–Phosphorus Dynamics in Sediments of a Coastal Hypoxic
643 Basin. *Environ. Sci. Technol.* **50**, 1227–1233.

644 Thomas M. R. and O'Shea E. K. (2005) An intracellular phosphate buffer filters transient
645 fluctuations in extracellular phosphate levels. *Proc. Natl. Acad. Sci.* **102**, 9565–9570.

Travis J. L. and Bowser S. S. (1991) The motility of Foraminifera. In *Biology of the Foraminifera* (eds. J. J. Lee and O. R. Anderson). Academic Press, London. pp. 91–155.

Veeh H. H., Burnett W. C. and Soutar A. (1973) Contemporary phosphorites on the continental margin of peru. *Science* **181**, 844–5.

Wallmann K. (2010) Phosphorus imbalance in the global ocean? *Global Biogeochem. Cycles* **24**, n/a-n/a.

Woehle C., Roy A.-S., Glock N., Wein T., Weissenbach J., Rosenstiel P., Hiebenthal C., Michels J., Schönfeld J. and Dagan T. (2018) A Novel Eukaryotic Denitrification Pathway in Foraminifera. *Curr. Biol.* **0**.

Figure captions:

Figure 1: Map with sampling locations. Crosses and circles indicate MUC and BIGO deployments, respectively. Sampling locations from Meteor cruise M137 are marked in black, while sampling locations from Meteor cruise M77 are marked in purple.

Figure 2: Living (rose-Bengal stained) benthic foraminifera form the Peruvian OMZ. **1:** *Bolivina interjuncta* (M137 - 788). **2:** *Bolivina seminuda* (M137 - 681). **3:** *Bolivina costata* (M137 - 681). **4:** *Bolivina plicata* (M137 - 608). **5:** *Globobulimina pacifica* (M137 - 670). **6:** *Nonionella auris* (M137 - 641). **7:** *Uvigerina striata* (M137 - 735). **8:** *Cassidulina limbata* (M137 - 608). **9:** *Valvulineria inflata* (M137 - 735). **10:** *Cancris carmenensis* (M137 - 608). The images were taken with a Keyence VHX-700 FD digital microscope at the Institute of Geosciences, Kiel University, Germany.

Figure 3: Comparison of nutrients extracted from benthic foraminifera, depending on whether the individuals were crushed or not before analysis. $[DIP]_i$ and $[NO_3^-]_i$ refer to the concentration of nutrients within the cytoplasm.

Figure 4: Examples of phosphatizing foraminifera in different stages between 640 and 928 m water observed at 11°S off Peru. **A**: *Cassidulina limbata* **B**: *Globobulimina pacifica* **C&D**: Abundant phosphorite grains in phosphoritic sands with the size and shape of foraminifera (grain size fraction 250-325 µm). **E**: Examples of various stages of foraminiferal phosphatization. The tests of the specimens are completely filled with phosphorites, as shown on similar samples from the same region (Manheim et al., 1975).

Figure 5: Log-log plot and power regression of DIP_i against cell volume of benthic foraminifera from the Peruvian OMZ. Error bars for the cell volumes are the standard error of the mean (1 SEM). Precision of the DIP_i measurements was 1%. Uncrushed samples of *B. costata* were also included, since the results were not different between the crushed and the uncrushed samples for this small species (see also figure 1).

Figure 6: Log-log plot and power regression of $NO_3^-{}_i$ against cell volume of benthic foraminifera from the Peruvian OMZ. Error bars for the cell volumes are the standard error of the mean (1 SEM). Precision of the NO_3^- measurements was 1%. Uncrushed samples of *B. costata* were also included, since the results were not different between the crushed and the uncrushed samples for this small species (see also figure 1).

Figure 7: The total benthic foraminiferal DIP pool in the sediment column in the Peruvian OMZ at 11°S (RV Meteor cruise M77) and 12°S (cruise M137). Error bars are 1sd and were calculated using propagation of uncertainty (for details see appendix 2). The grey area indicates water depths where abundant phosphorites with encrusted foraminifera have been reported (Resig and Glenn, 1997).

694 Table 1: Sampling sites. “BIGO” indicates that the sediment was retrieved with a benthic lander
695 after in situ incubation of the sediment for ~ 36 h (e.g. Sommer et al., 2016). At all other sites the
696 sediment was retrieved with a video guided multiple-corer (MUC).

Station	Latitude (S)	Longitude (W)	Depth (m)
M137 - 642 BIGO2-2	12°14.89'	77°12.70'	102
M137 - 656 BIGO1-2	12°16'37'	77°14.95'	128
M137 - 696 BIGO1-3	12°21.51'	77°21.71'	193
M137 - 608 MUC 4	12°23.26'	77°24.28'	244
M137 - 641 MUC 7	12°16.68'	77°14.99'	128
M137 - 670 MUC 12	12°31.36'	77°35.00'	752
M137 - 681 MUC 13	12°13.51'	77°10.77'	74
M137 - 695 MUC 17	12°16.78'	77°14.98'	130
M137 - 735 MUC 24	12°38.14'	77°20.74'	489
M137 - 756 MUC 27	12°23.25'	77°24.27'	242
M137 - 776 MUC 32	12°24.90'	77°26.29'	303
M137 - 788 MUC 34	12°27.20'	77°29.30'	413
M137 - 813 MUC 27	12°23.29'	77°24.27'	242
M137 - 825 MUC 38	12°21.50'	77°21.71'	193
M137 - 826 MUC 39	12°24.90'	77°26.28'	301
M137 - 838 MUC 41	12°13.47'	77°10.86'	75
M137 - 841 MUC 44	12°17.01'	77°14.70'	130
M137 - 858 MUC 46	12°27.20'	77°29.51'	410

697

698

699 Table 2: Best resembling shapes for the biovolume determination of foraminiferal species used
700 in this study.

Species	Shape
Bolivina costata	Cone
Bolivina plicata	Cone
Bolivina interjuncta	Cone
Bolivina seminuda	Cone
Bolivina spissa	Cone with elliptic base
Cancris carmenensis	Prolate spheroid
Cassidulina limbata	Tri-axial elipsoid
Globobulimina pacifica	Prolate spheroid
Nonionella auris	Prolate spheroid
Uvigerina striata	Prolate spheroid
Valvulineria inflata	Prolate spheroid

701

702

703 Table 3: Mean individual intracellular DIP content for five foraminiferal species from the
704 Peruvian OMZ.

Species	mean DIP_i (pmol ind^{-1})	1sd
B. costata	33	4
B. interjuncta	321	45
B. seminuda	69	25
C. limbata	290	7
V. inflata	2603	684

705

706

Table 4: Number of individuals of foraminiferal species with known intracellular DIP content or intracellular DIP estimated from the average biovolume of the species in relation to the total foraminiferal abundances at the station.

Station	# individuals from species with known intracellular DIP (%)
M137 – 681 MUC 13	98
M137 – 641 MUC 7	75
M137 – 695 MUC 17	82
M137 – 608 MUC 4	68
M137 – 776 MUC 32	49
M137 – 788 MUC 34	24
M137 – 735 MUC 24	71
M137 – 670 MUC 12	8
M77/1-540 MUC-49	75
M77/1-583 MUC-65	95
M77/1-473 MUC-32	98
M77-1-449 MUC-19	89
M77/1-456 MUC-22	75
M77/1-459 MUC-25	19

Table 5: Mean biovolumes and intracellular nutrient content in benthic foraminifera from the Peruvian OMZ determined during M137. Intracellular DIP and NO_3^--contents are reported as individual specific (total content per individual, pmol ind^{-1}) and volume specific (intracellular content, mmol L^{-1}). ' # Ind.' refers to the number of specimens used for each analysis. Samples marked with an asterisk (*) were not crushed before analysis. SEM is the standard error of the mean.

Station	Species	Water depth (m)	# Ind.	Mean cell volume (μm^3)	1sem	DIP (pmol ind^{-1})	NO_3^- (pmol ind^{-1})	$[DIP]_i$ (mmol L^{-1})	$[NO_3^-]_i$ (mmol L^{-1})
642	*B. seminuda**	102	42	$1.71 \cdot 10^6$	6.73E+04	32	n.d.	19	n.d.
642	*B. seminuda**	102	85	$1.68 \cdot 10^6$	4.87E+04	34	28	20	17
642	*B. costata**	102	43	$7.60 \cdot 10^5$	3.28E+04	37	27	48	36
642	*B. costata**	102	80	$8.18 \cdot 10^5$	2.29E+04	31	42	38	51
656	*B. seminuda**	128	40	$1.65 \cdot 10^6$	4.58E+04	8	57	5	34
696	*C. limbata**	193	21	$1.14 \cdot 10^7$	1.02E+06	7	n.d.	1	n.d.
696	*B. seminuda**	193	64	$1.30 \cdot 10^6$	6.07E+04	13	7	10	6
756	*C. limbata*	242	22	$1.80 \cdot 10^7$	9.02E+05	294	2275	16	127
756	*C. limbata*	242	20	$2.12 \cdot 10^7$	1.14E+06	285	1949	13	92
756	*B. seminuda*	242	130	$1.40 \cdot 10^6$	4.02E+04	55	395	39	282
788	*V. inflata*	413	21	$1.42 \cdot 10^8$	1.43E+07	2516	24447	18	172
788	*V. inflata*	413	21	$1.50 \cdot 10^8$	1.24E+07	2294	24247	15	162
788	*B. interjuncta*	413	20	$1.62 \cdot 10^7$	1.20E+06	285	717	18	44
788	*B. interjuncta*	413	18	$1.60 \cdot 10^7$	1.18E+06	371	1403	23	88
813	*B. seminuda**	242	40	$1.54 \cdot 10^6$	7.81E+04	38	82	25	53
813	*B. seminuda*	242	40	$1.54 \cdot 10^6$	6.63E+04	37	89	24	58
825	*B. seminuda*	193	35	$1.67 \cdot 10^6$	7.46E+04	79	417	47	250
825	*B. seminuda*	193	46	$1.52 \cdot 10^6$	7.08E+04	65	255	43	168
826	*V. inflata*	301	12	$8.78 \cdot 10^7$	1.09E+07	2019	2013	23	23
826	*B. seminuda*	301	40	$2.48 \cdot 10^6$	9.32E+04	113	110	46	44
838	*B. costata*	75	94	$7.99 \cdot 10^5$	1.83E+04	30	34	37	43
841	*B. seminuda*	130	38	$1.55 \cdot 10^6$	7.35E+04	65	97	42	63
858	*V. inflata*	410	8	$1.62 \cdot 10^8$	1.93E+07	3582	19957	22	123
858	*B. interjuncta*	410	20	$1.47 \cdot 10^7$	1.06E+06	308	1598	21	109

Table 6: Mean cell volumes of six additional benthic foraminiferal species from the Peruvian OMZ for which intracellular nutrient content was not measured. DIP_i for these species were calculated from the mean cell volumes using eq. 5. The error in DIP_i (σ_{DIPi_β}) was calculated using propagation of uncertainty. Positive and negative sds differ due to non-linearity of the power correlation. See Appendix 2 for a detailed definition of σ_{DIPi_β} and details about the propagation of uncertainty.

Species	ind.	mean cell volume (μm^3)	1sem	DIP_i (pmol ind^{-1}) calc. with Eq.5	$\ln(\sigma_{DIPi_\beta})$	σ_{DIPi_β} 1sd (pmol ind^{-1})
B. plicata	24	4.20E+06	3.48E+05	128	0.70	+129/-64
B. spissa	38	4.62E+06	2.18E+05	139	0.70	+140/-70
C. carmenensis	13	4.96E+07	8.44E+06	973	0.76	+1100/-516
G. pacifica	2	1.12E+08	2.19E+07	1900	0.78	+2230/-1030
N. auris	25	2.66E+06	2.97E+05	88	0.69	+88/-44
U. striata	22	2.68E+07	2.44E+06	587	0.73	+636/-305

734 Table 7: Estimated total benthic foraminiferal DIP storage at different sampling sites from two different transects in the Peruvian
735 OMZ. $\Sigma DIP_{i\ sed\ tot}$ is the total DIP in the sediment column stored in foraminifera (in mmol m^{-2}). $[DIP]_{i\ sed\ tot}$ is the total sedimentary
736 intracellular [DIP], and $[DIP]_{i\ sed\ tot}$ are mean values for the top 3 cm of sediment (M137) or the first cm of sediment (M77).
737 Foraminiferal abundances are also listed. Abundances from M77 were taken from (Glock et al., 2013). The errors $\sigma_{DIPi\ sed\ tot}$ and
738 $\sigma_{[DIP]i\ sed\ tot}$ were calculated using propagation of uncertainty. Positive and negative sds differ due to non-linearity of the power
739 correlation. See Appendix 2 for details about the propagation of uncertainty.

Station	Water depth (m)	Longitude (°W)	Latitude (°S)	Foraminiferal abundance (ind cm^{-2})	$\Sigma DIP_{i\ sed\ tot}$ (mmol m^{-2})	$\sigma_{DIPi\ sed\ tot}$ (mmol m^{-2}) 1sd	$[DIP]_{i\ sed\ tot}$ (µmol l^{-1} of wet sediment)	$\sigma_{[DIP]i\ sed\ tot}$ (µmol l^{-1} of wet sediment) 1sd
M137 – 681 MUC 13	74	77°10.77'	12°13.51'	1455.9	0.55	+0.09/-0.07	21	+3/-3
M137 – 641 MUC 7	128	77°14.99'	12°16.68'	569.9	0.40	+0.17/-0.16	20	+8/-8
M137 – 695 MUC 17	130	77°14.98'	12°16.78'	644.6	0.48	+0.18/-0.18	18	+7/-7
M137 – 608 MUC 4	244	77°24.28'	12°23.26'	10.4	0.01	+0.01/-0.00	1	+0/-0
M137 – 776 MUC 32	303	77°26.29'	12°24.90'	410.2	0.53	+0.27/-0.24	20	+10/-9
M137 – 788 MUC 34	413	77°29.30'	12°24.90'	1061.7	3.48	+2.25/-2.14	137	+89/-85
M137 – 735 MUC 24	489	77°20.74'	12°24.90'	372.0	1.52	+0.91/-0.61	78	+47/-31
M137 – 670 MUC 12	752	77°35.00'	12°24.90'	25.4	0.14	+0.11/-0.10	5	+4/-4
M77/1-540 MUC 49	79	77°47.40'	11°00.01'	343.7	0.10	+0.03/-0.03	7	+3/-3
M77/1-583 MUC 65	248	78°03.06'	11°06.86'	616.2	0.46	+0.17/-0.16	43	+15/-15
M77/1-473 MUC 32	317	78°09.94'	11°00.01'	522.5	0.60	+0.17/-0.12	119	+34/-25
M77-1-449 MUC 19	319	78°09.97'	11°00.01'	262.4	0.47	+0.21/-0.13	94	+42/-27
M77/1-456 MUC 22	465	78°19.23'	11°00.01'	61.3	0.25	+0.23/-0.23	25	+8/-7
M77/1-459 MUC 25	697	78°25.60'	11°00.03'	12.7	0.03	+0.03/-0.02	3	+3/-2

740

Figure 1

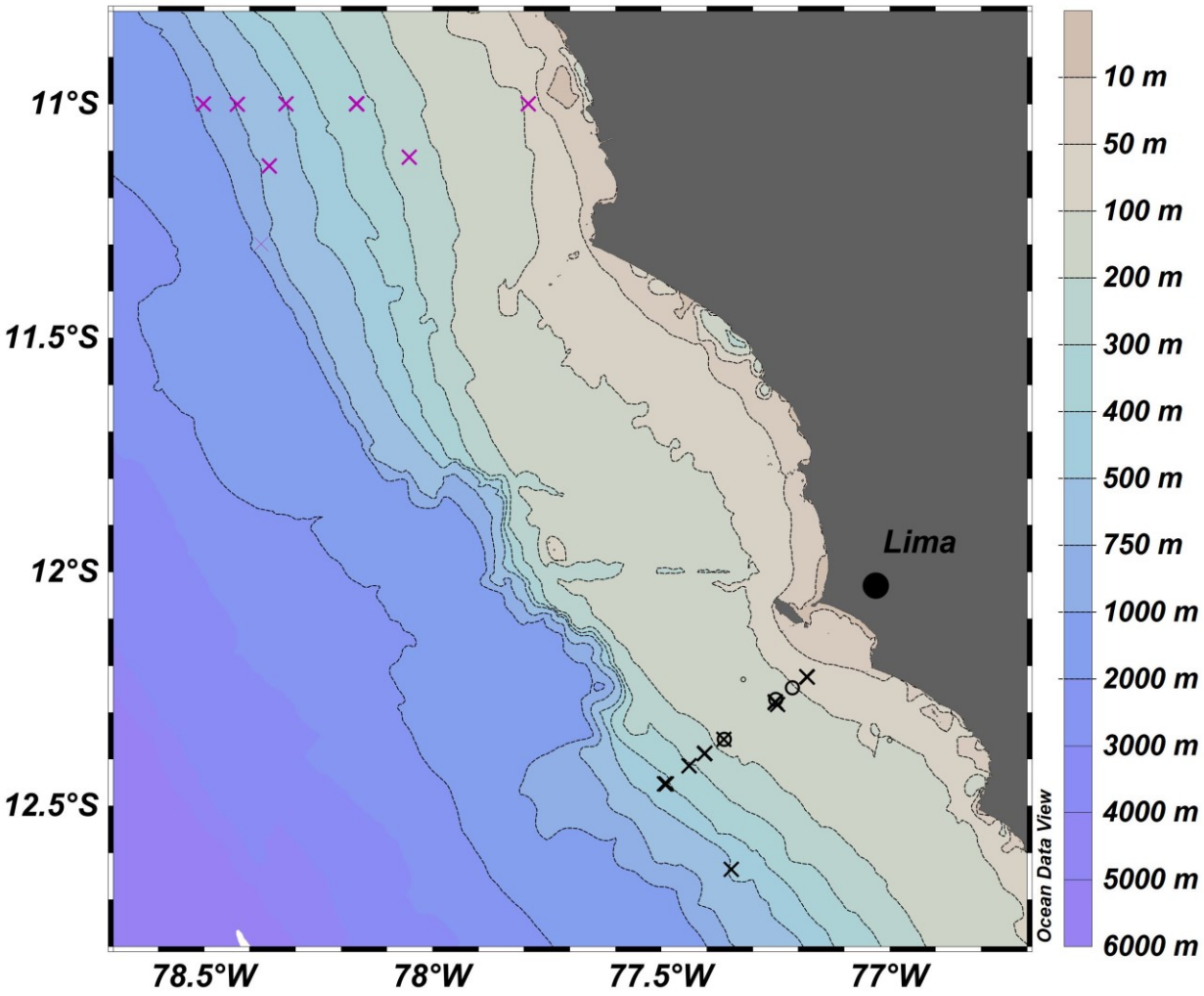
11°S
11.5°S
12°S
12.5°S
78.5°W
78°W
77.5°W
77°W
Lima
Ocean Data View
10 m
50 m
100 m
200 m
300 m
400 m
500 m
750 m
1000 m
2000 m
3000 m
4000 m
5000 m
6000 m

Figure 2

Figure 3

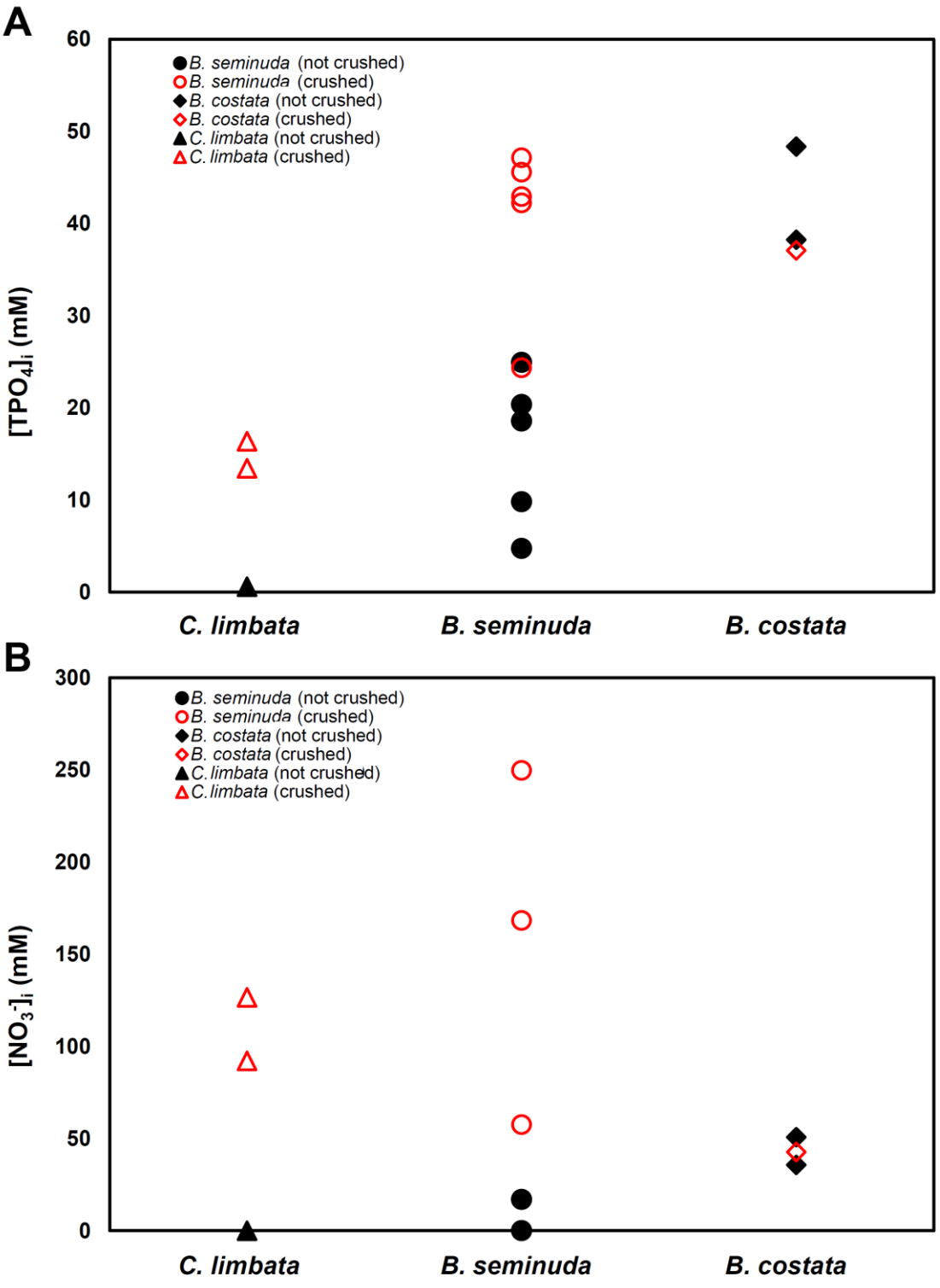
A
60
50
40
30
20
10
0
[TPO4]i (mM)
B. seminuda (not crushed)
B. seminuda (crushed)
B. costata (not crushed)
B. costata (crushed)
C. limbata (not crushed)
C. limbata (crushed)
C. limbata
B. seminuda
B. costata
B
300
250
200
150
100
50
0
[NO3-]i (mM)
B. seminuda (not crushed)
B. seminuda (crushed)
B. costata (not crushed)
B. costata (crushed)
C. limbata (not crushed)
C. limbata (crushed)
C. limbata
B. seminuda
B. costata

Figure 4

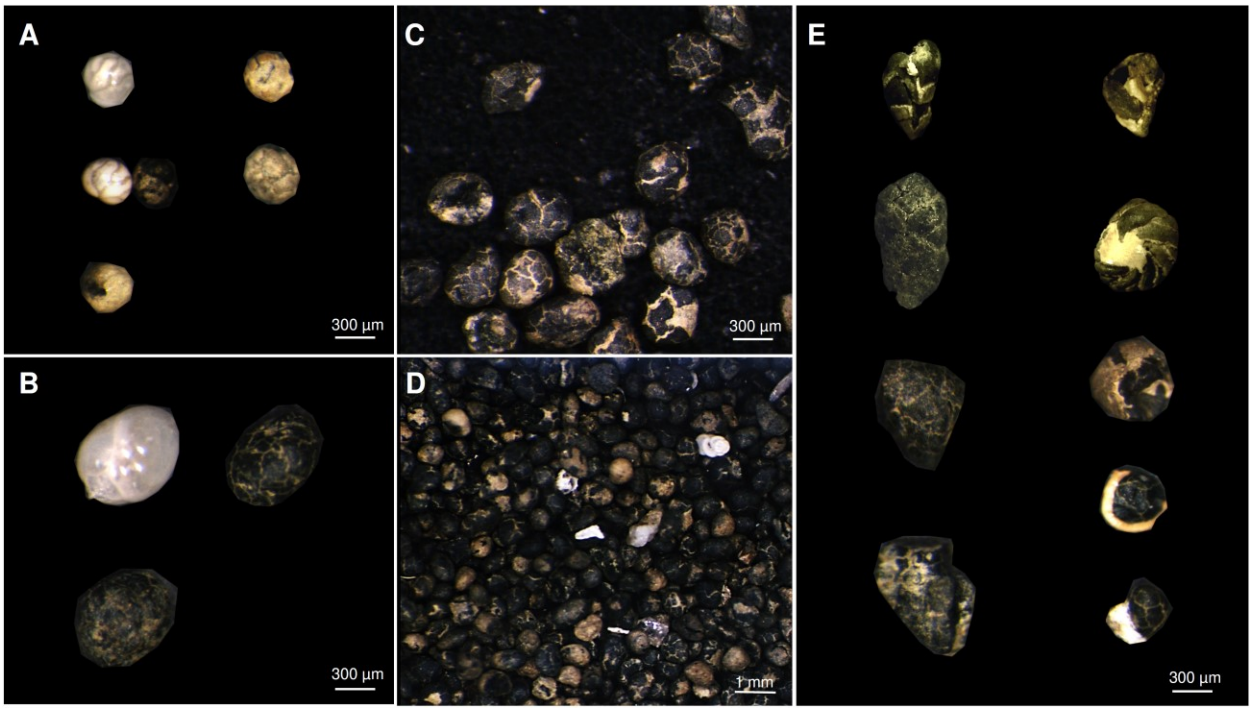

Figure 5

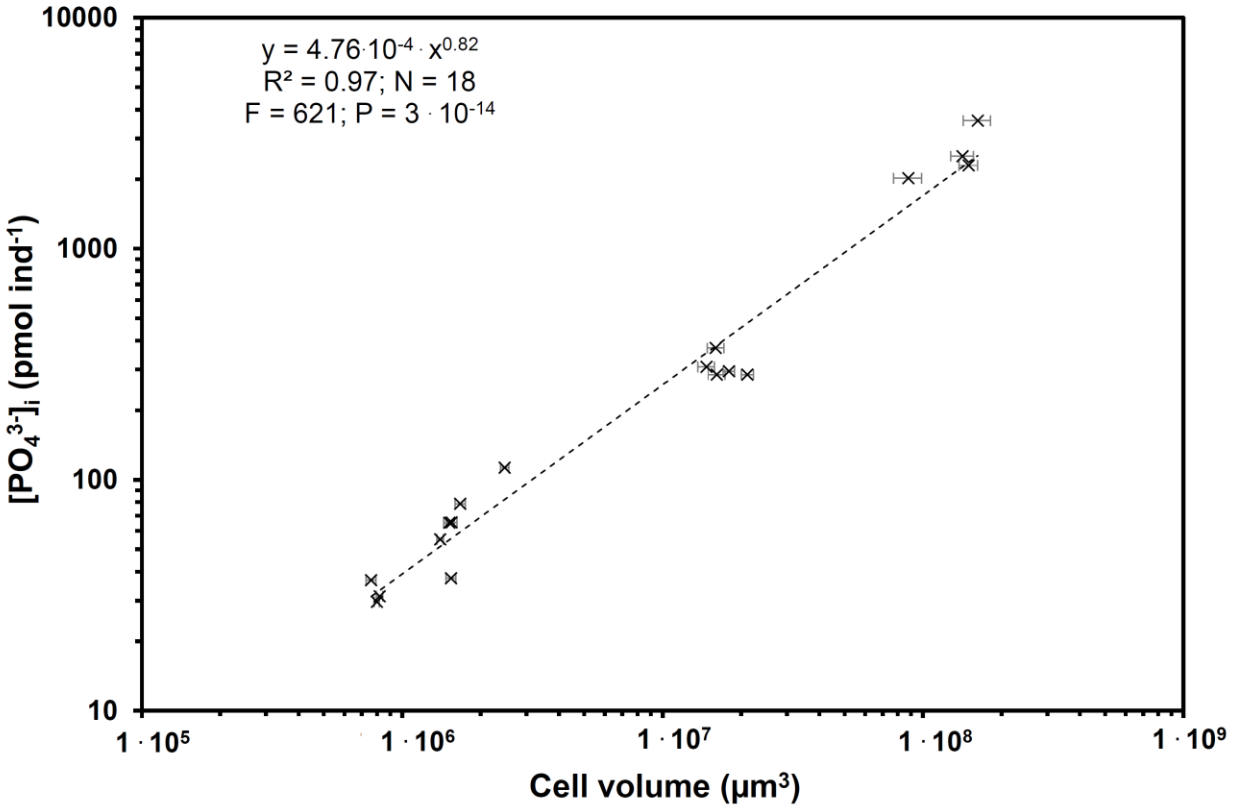
y = 4.76·10-4 · x0.82
R² = 0.97; N = 18
F = 621; P = 3 · 10-14
10000
1000
100
10
[PO43-]i (pmol ind-1)
1 · 10⁵
1 · 10⁶
1 · 10⁷
1 · 10⁸
1 · 10⁹
Cell volume (µm³)

Figure 6

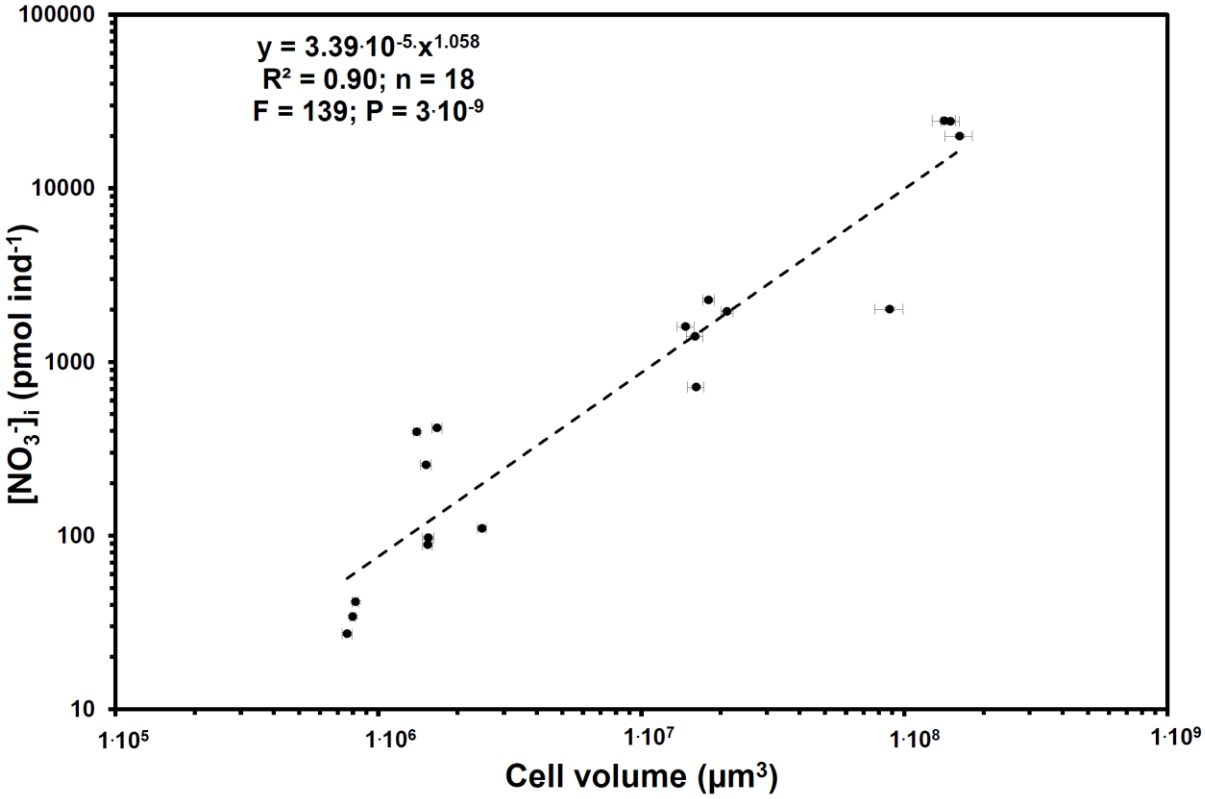
y = 3.39·10-5·x1.058
R² = 0.90; n = 18
F = 139; P = 3·10-9
100000
10000
1000
100
10
[NO3-]i (pmol ind-1)
1·10⁵
1·10⁶
1·10⁷
1·10⁸
1·10⁹
Cell volume (µm³)

Figure 7

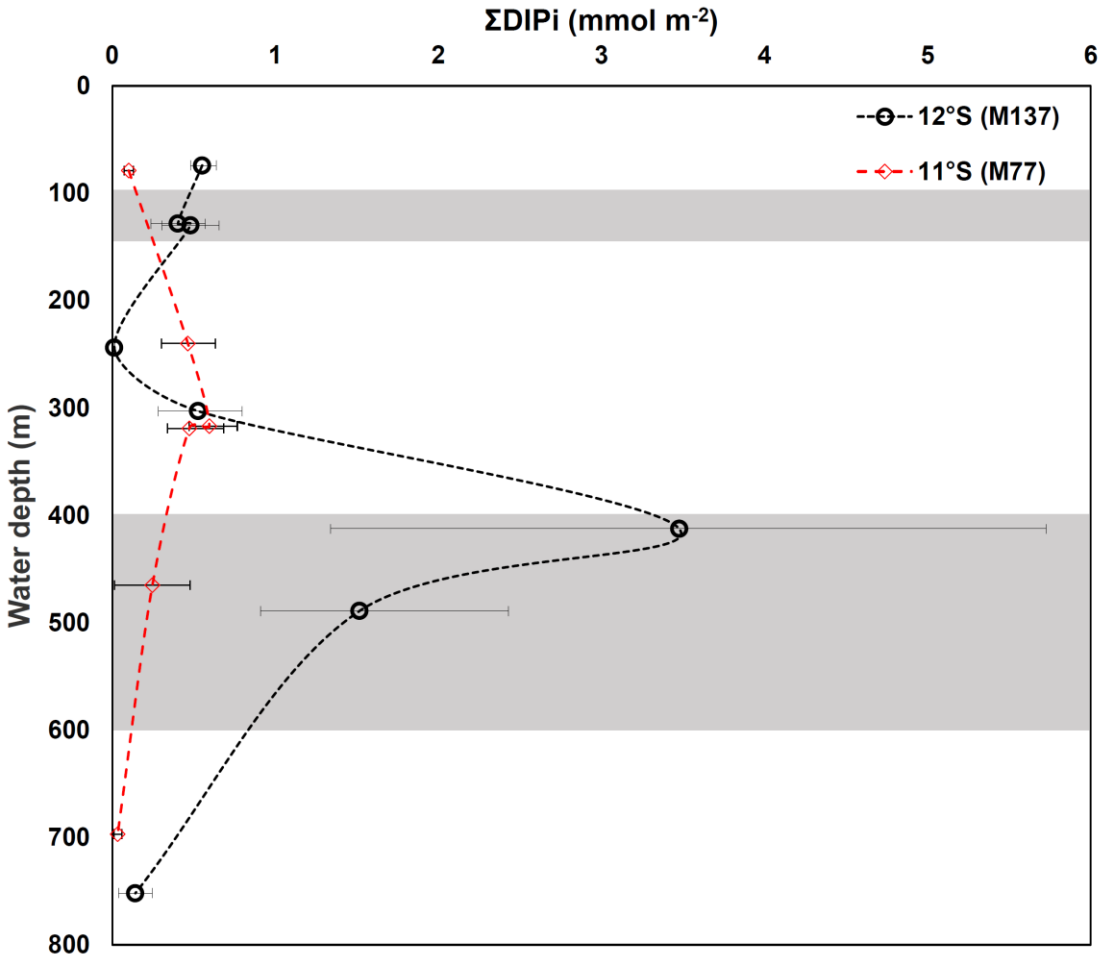
ΣDIPi (mmol m-2)
0
1
2
3
4
5
6
Water depth (m)
0
100
200
300
400
500
600
700
800
12°S (M137)
11°S (M77)

Appendix 1: Taxonomic references

Benthic foraminiferal species from the Peruvian OMZ were determined using recent literature from the study area (Mallon, 2011, Erdem, 2016, Figueora et al., 2005), and earlier, regional studies from the western Pacific (Uchio 1960, Boltovskoy and Theyer, 1970, Ingle et al., 1980, Resig 1981, 1990). The taxonomy was cross-checked with the type figures and references retrieved from the Ellis and Messina (1940-2014) catalogue. The validity of the genera was assessed after Loeblich and Tappan (1988). Specimen images on Plate 1 are given in square brackets.

Bolivina costata d'Orbigny 1839, p. 62, pl. 8, figs. 8-9 [fig. 3].

Bolivina interjuncta Cushman 1926 = *Bolivina costata* d'Orbigny var. *interjuncta* Cushman, p. 41, pl. 6, fig. 3 [fig. 1].

Bolivina plicata d'Orbigny 1839, p. 62, pl. 8, figs. 4-7 [fig. 4].

Bolivina seminuda Cushman 1911, p. 34, fig. 55 [fig. 2]. Note: the flush sutures, the smooth surface, and the numerous pores in the lower half of each chamber, giving the lower part of the chamber wall a frothy appearance, are characteristic features of this species.

Bolivina spissa Cushman 1926 = *Bolivina subadvena* Cushman var. *spissa* Cushman, p. 45, pl. 6, fig. 8.

Cancris carmenensis Natland 1950, p. 32, pl. 9, fig. 1 [fig, 10]. Note: broad, inflated chambers, depressed sutures, and a knob formed by the early chambers in the centre of the spiral side are distinctive features of this species. The youngest chambers of small specimens may be rather high, successive in arrangement rather than over-arching, and their margin may be slightly acute. They were also observed gathering long silica spicules in the detritus cyst before their aperture, probably to stabilize their pseudopodial network (Lutze and Altenbach 1988). Such specimens have been determined as *C. auriculus* or *Valvulina oblonga* (Figueroa et al., 2005; Mallon, 2011; Erdem, 2016), even though the Peruvian Margin morphotypes do not show a distinct keel and their chamber wall is much thicker as compared to the genuine *C. auriculus* from the northern Atlantic.

Cassidulina limbata Cushman and Hughes 1925, p. 12, pl. 2, fig. 2 [fig, 8]. Note: The "pinched-in" narrowing in the middle part of the chambers are unique to this species. The closely related *C. auka* Boltovskoy and Theyer 1970 differs from *C. limbata* by its higher number of chambers per whorl, the marked sutural ridges, the elevated umbilical boss, and the triangular apertural aspect.

Globobulimina pacifica Cushman 1927, p. 67, pl. 14, fig. 12 [fig. 5].

Nonionella auris (d'Orbigny 1839) = *Valvulina auris* d'Orbigny, p. 47, pl. 2, figs. 15-17 [fig. 6]. Note: numerous chambers, a lobate outline, and the very thin and sigmoidal extension of the last chamber covering the umbilicus are diagnostic features of this species.

Uvigerina striata d'Orbigny 1839, p. 53, pl. 7, fig. 16 [fig. 7].

Valvulineria inflata (d'Orbigny 1839) = *Valvulina inflata* d'Orbigny, p. 48, pl. 7, figs. 7-9 [fig. 9].

Appendix 2: Propagation of uncertainty for the sedimentary DIP stored in foraminifera

For the calculation of the errors for $\Sigma DIP_{i\ sed\ tot}$ and $[DIP]_{i\ sed\ tot}$ a complete error propagation has been applied including three different kinds of error. The first error is the 1sd we have for the DIP_i for the five species directly measured (see Tab. 3). This error is defined as $\sigma_{DIPi\alpha}$ in pmol ind^{-1}.

The second type of error concerns the species for which we determined the mean biovolume (Tab. 6) and the DIP_i estimated using Eq.6. We define this error as σ_{DIPi_β} It includes the error for the mean cell volumes (1SEM; see tab. 6). This error is defined as σ_{Vcell}. Eq.6 in the main manuscript is given in the form of:

Eq. A1 $$\ln(DIP_i) = a \cdot \ln(V_{cell}) + b$$

A propagation of uncertainty on Eq.A1, results in the following equation:

Eq. A2: $$\ln(\sigma_{DIPi_\beta}) = \sqrt{\left(\frac{\partial DIP_i}{\partial a}\right)^2 \cdot \sigma_a^{\ 2} + \left(\frac{\partial DIP_i}{\partial b}\right)^2 \cdot \sigma_b^{\ 2} + \left(\frac{\partial DIP_i}{\partial V_{cell}}\right)^2 \cdot \sigma_{Vcell}^{\ 2}}$$

Solution of the derivatives in Eq. A2 and the use of errors and constants of Eq.6 results in

Eq. A3: $$\ln(\sigma_{DIPi_\beta}) = \sqrt{\ln(V_{cell})^2 \cdot 0.03^2 + 0.52^2 + \left(0.82 \cdot \frac{1}{V_{cell}}\right)^2 \cdot \sigma_{Vcell}^{\ 2}}$$

Note that this results in different positive and negative values for σ_{DIPi_β} after transformation of $\ln(\sigma_{DIPi_\beta})$ due to the non-linearity of the power function. The positive error is defined according to Eq.A4:

Eq. A4 $$\sigma_{DIPi_\beta}(positive) = exp^{\ln(DIP_i)+\ln(\sigma_{DIPi_\beta})} - DIP_i$$

The negative error is defined according to Eq.A5

Eq. A5 $$\sigma_{DIPi_\beta}(negative) = DIP_i - exp^{\ln(DIP_i)-\ln(\sigma_{DIPi_\beta})}$$

A propagation of uncertainty of these factors applied to Eq.1 of the main manuscript results in the following equation for $\sigma_{\Sigma DIPi\ sed.}$(in mmol m^{-2}):

Eq. A6 $$\sigma_{\Sigma DIPi\ sed} = 10^{-9}\sqrt{\sum(A_{n\alpha})^2 \cdot (\sigma_{DIPi\alpha n})^2 + \sum(A_{n\beta})^2 \cdot (\sigma_{DIPi\beta n})^2}$$

Where $A_{n\alpha}$ is the abundance of the foraminiferal species n for which we measured mean intracellular DIP_i and A_{n_β} is the abundance of the foraminiferal species n for which we calculated DIP_i, using their mean cell volume according to Eq. 5 of the main manuscript. $\sigma_{DIPi\alpha n}$ and $\sigma_{DIPi\beta n}$

are the corresponding $\sigma_{DIPi\alpha}$ and $\sigma_{DIPi\beta}$ for the species n. Note that the factor of 10^{-9} has to be applied to convert pmol to mmol.

In the same way a propagation of uncertainty applied to Eq.2 of the main manuscript results in the following equation for $\sigma_{[DIP]i\ sed}$ (in mmol L^{-1} of wet sediment):

$$\text{Eq. A7} \qquad \sigma_{[\mathrm{DIP}]\mathrm{i\ sed}} = 10^{-9}\sqrt{\sum(PD_{n\alpha})^2 \cdot (\sigma_{DIPian})^2 + \sum(PD_{n\beta})^2 \cdot (\sigma_{DIPi\beta n})^2}$$

where $PD_{n\alpha}$ is the population density of the foraminiferal species n for which we measured mean intracellular DIP_i and PD_{n_β} is the abundance of the foraminiferal species n for which we calculated DIP_i, using their mean cell volume according to Eq. 5 of the main manuscript.

Negative and positive errors have to be calculated separately for Eq. A6 and Eq. A7 according to equations Eq. A4 and Eq. A5 due to the non-linearities.

Note that the errors of abundances and population densities have to be neglected within this error propagation because these are not known, since no replicates were done for the determination of the living foraminiferal assemblages, according to the high workload related to this task. Previous studies showed that population densities of sample replicates, which have been picked dry by a single investigator had an accuracy (1σ) of ±2 % (Schönfeld et al., 2013). This should be negligible in comparison to the other errors within this propagation of uncertainty.

The largest uncertainty in $\Sigma DIP_{\mathrm{i\ sed\ tot}}$ (Eq.3 main manuscript) and $[TDP]_{\mathrm{i\ sed\ tot}}$ (Eq. 4 main manuscript) arises from the percentage of the species for which neither cell volume nor DIP_i was measured. These species are now defined as species *nγ*. We do not know this factor but assume that the relative uncertainty can be up to ~±75%. Thus the higher the proportion of the species *nγ* is, the higher is the total uncertainty of the of the DIP_i reservoir in the sediments. Therefore, for the uncertainties $\sigma_{\Sigma DIP_{\mathrm{i\ sed\ tot}}}$ the following term was added to $\sigma_{\Sigma DIPi\ sed.}$:

$$\text{Eq. A8} \qquad 0.75 \cdot (\Sigma DIP_{\mathrm{i\ sed\ tot}} - \Sigma DIP_{\mathrm{i\ sed}})$$

and accordingly for the uncertainties of $\sigma_{[TDP]_{\mathrm{i\ sed\ tot}}}$ the following term was added to $\sigma_{[DIP]i\ sed:}$

$$\text{Eq. A9} \qquad 0.75 \cdot ([TDP]_{\mathrm{i\ sed\ tot}} - [TDP]_{\mathrm{i\ sed}})$$

Thus, if a proportion of 50% belonged to species *nγ*, an error of $\pm 50 \cdot 0.75 = \pm 37.5\%$ would be added. For a hypothetic total benthic foraminiferal DIP pool in the sediment column ($\Sigma DIP_{\mathrm{i\ sed\ tot}}$) of 1 mmol m^{-2} with a proportion of 50% belonging to species *nγ* within the assemblages, an uncertainty of ± 0.375 mmol m^{-2} was added to $\sigma_{\Sigma DIPi\ sed}$ from Eq. A6.

This exercise demonstrates that knowledge about sedimentary intracellular stored DIP can be improved with more measurements on foraminiferal cell volume or, preferably, species specific DIP_i in foraminiferal assemblages.

References (Appendix)

Boltovskoy E. and Theyer F. (1970) Foraminíferos recientes de Chile central. Homenaje al doctor Angel Gallardo. Revista del Museo Argentino de Ciencias Naturales "Bernardino Rivadavia" e Instituto Nacional de Investigación de las Ciencias Naturales. *Hidrobiol*. **2**, 279–379.

Cushman J. A. (1911) A monograph of the foraminifera of the North Pacific Ocean, Part 2, Textulariidae. *United States Nat. Mus. Bull*. **71**, 1–108.

Cushman J. A. (1926) Some Pliocene Bolivinas from California. *Contr. Cushman Lab. Foram. Res*. **2**, 40–47.

Cushman J. A. (1927) An outline of the re-classification of the foraminifera. *Contr. Cushman Lab. Foram. Res*. **3**, 1–105.

Cushman J. A. and Hughes D. D. (1925) Some later Tertiary Cassidulinas of California. *Contr. Cushman Lab. Foram. Res*. **1** 11–17.

d'Orbigny A. D. (1839) *Voyage dans l'Amérique méridionale – Foraminifères*, vol. 5, pt. 5, Levrault, Strasbourg, France.

Ellis B. F. and Messina A. (1940-2014) *Cataloque of foraminifera*. Micropaleontology Press, New York. Available from: http://www.micropress.org (Date of last access: 13-03-2019).

Erdem Z. (2016) *Reconstruction of past bottom water conditions of the Peruvian Oxygen Minimum Zone for the last 22,000 years and the benthic foraminiferal response to (de)oxygenation*. Dissertation, Christian-Albrechts-Universität zu Kiel, Kiel, Germany.

Figueroa S., Marchant M., Giglio S. and Ramírez M. (2005) Foraminiferos bentonicos rotalinidos del centro sur de Chile (36°S - 44°S). *Gayana* **69**, 329–363.

Ingle J. C., Keller G. and Kolpack R. L. (1980) Benthic foraminiferal biofacies, sediments and water masses of the southern Peru-Chile Trench area, southeastern Pacific Ocean. *Micropaleontol*. **26**, 113–150.

Loeblich A. R. and Tappan H. (1988) *Foraminiferal Genera and their Classification*. Van Nostrand Reinhold, New York.

Lutze G. F. and Altenbach A. V. (1988) *Rupertina stabilis* (Wallich), a highly adapted, suspension feeding foraminifer. *Meyniana* **40**, 55–69.

Mallon J. (2011) *Benthic foraminifera of the Peruvian and Ecuadorian continental margin*. Dissertation, Christian-Albrechts-Universität zu Kiel, Kiel, Germany.

Natland M. L. (1950) The 1940 E.W. Scripps Cruise to the Gulf of California, Part IV. Report on the Pleistocene and Pliocene Foraminifera. *Mem. Geol. Soc. America* **43**, 1–55.

Resig J. M. (1981) Biogeography of benthic foraminifera of the northern Nazca plate and adjacent continental margin. *Mem. Geol. Soc. America* **154**, 619–644.

Resig J. M. (1990) Benthic foraminiferal stratigraphy and paleoenvironments off Peru leg 112. *Proc. Ocean Drilling Program, Sci. Res*. **112**, 263–296.

Schönfeld, J., Golikova, E., Korsun, S. and Spezzaferri, S.: The Helgoland Experiment – assessing the influence of methodologies on Recent benthic foraminiferal assemblage composition, J. Micropalaeontology, 32(2), 161–182, doi:10.1144/jmpaleo2012-022, 2013.

Uchio T. (1960) Ecology of living benthonic foraminifera from the San Diego, California area. Spec. Pub. Cushman Found. Foram. Res. **5**, 1–72.

1 Table A1: Population densities and abundances of living benthic foraminifera.

Station	M137 - 681	M137 - 641	M137 - 695	M137 - 608	M137 - 776	M137 - 788	M137 - 735	M137 - 670
Sampling date	12.05.2017	09.05.2017	13.05.2017	07.05.2017	19.05.2017	20.05.2017	16.05.2017	11.05.2017
Time (UTC)	17:36	19:45	18:42	14:53	19:10	15:50	14:23	23:22
Depth (m)	74	128	130	244	303	413	489	752
Sample	0-3 cm	0-3 cm (composite)	0-3 cm	0-3 cm (composite)	0-3 cm	0-3 cm	0-3 cm	0-3 cm
Alabaminella weddellensis								4
Alliatina primitiva				9.1	6	1	20	
Ammodiscus minutissimus				1	1			
Ammomarginulina catenulata								17
Anomalinoides minimus				1				
Arenoparella oceanica		1		1	1	3		
Bathysiphon capillare							1	
Bolivina alata							4	
Bolivina costata	650	49.2	40	2.1	1			
Bolivina interjuncta						6	42	
Bolivina pacifica	1	26.7	16	59.9	17	3	3	2
Bolivina plicata		6		10.1	36	27	40	1
Bolivina seminuda	56	387.6	277	236.8	86	15	52	2
Bolivina spissa							3	6
Bolivina subadvena							5	
Bolivinita minuta							4	17
Buccella peruviana	4							
Buliminella curta					7	5	7	37
Buliminella elegantissima	4	6.1	5	9.1	17			
Buliminella tenuata							1	4
Cancris carmenensis				8.3	1	4	42	3
Cassidulina crassa								7
Cassidulina laevigata								18
Cassidulina limbata		5	2	34.8	27	3	16	
Chilostomella ovoidea							1	
Cribrostomoides crassimargo								1
Eggerella humboldti								2
Eggerella pusilla							2	
Eggerella scrippsi		1		5.6	3			
Eggerelloides scaber							1	
Epistominella afueraensis		41.1	17	9.3	5	1		

Epistominella obesa					4	60		
Fursenkoina cornuta							3	
Fursenkoina glabra	5	88.3	37	32	31	3		
Globobulimina pacifica								2
Globocassidulina subglobosa								2
Gyroidina soldanii					1	1	4	
Haplophragmoides evoluta				0.5	1	2	2	2
Hoeglundina elegans							2	2
Leptohalysis gracilis							1	
Nonionella auris	34	36.7	14					
Nonionella turgida								3
Nonionides grateloupi								11
Reophax bilocularis								1
Reophax calcareus								1
Spiroplectammina biformis					1			
Suggrunda eckisi				2.6	30	29	7	
Suggrunda kleinpelli				5.1	14	19		
Suggrunda porosa				1.1	17	58	24	
Trifarina angulosa								5
Portatrochammina pacifica						1		1
Pseudolachlanella slitella								1
Quinqueloculina seminulum								2
Uvigerina peregrina								9
Uvigerina striata							27	
Valvulineria glabra								7
Valvulineria inflata			1			3	3	
others								
Total	754	648.7	409	429.4	307	244	317	170
Species number	7	11	9	18	21	19	26	28
Surface area (cm^2)	6.7	78.5	6.7	78.5	6.7	6.7	6.7	6.7
Volume (cm^3)	18	153	18	96	18	17	13	19
Split (n)	0.0773	0.0145	0.0947	0.5276	0.1117	0.0343	0.1272	1.0000
Population density (Ind./1 cm^3)	542	292	240	8	153	418	192	9
Total abundance (Ind./ 1 cm^2)	1456	570	645	10	410	1062	372	25
Fisher's alpha	1.1	1.9	1.6	3.8	5.1	4.8	6.7	9.5

2

3